Received: 20 October 2022 | Revised: 16 February 2023 | Accepted: 7 May 2023

DOI: 10.1002/eqe.3921

RESEARCH ARTICLE

WILEY

# Haunch retrofit of RC beam–column joints: Linear stress field analysis and Strut-and-Tie method application

**Angelo Marchisella** | **Giovanni Muciaccia**

Department of Civil and Enviromental Engineering, Politecnico di Milano, Milan, Italy

**Correspondence**
Angelo Marchisella.
Email: angelo.marchisella@polimi.it

**Abstract**

This paper addresses the stress field of reinforced concrete (RC) beam–column joints retrofitted with haunches. Design of such solution currently assumes internal forces evaluated by the so called $\beta$-factor approach, which was originally conceived targeting the enhancement of steel moment-resisting frames. Extension to RC is subsequent as it emerges from the literature survey. The analytical model is first critically rediscussed. Inconsistencies of the adopted structural scheme, with respect to the actual mechanical behavior, may lie on the compatibility conditions which are imposed between the haunch and concrete beam (or column). In this regard, two-dimensional finite element models (FEM), using linear-elastic materials, are employed to study the stress field of two benchmark specimens derived from literature. A partial validation is carried out against experimentally derived internal forces. Results show that, for haunches with extended flat plates and stiff diagonals, compressive diffusion affects the entire haunch region. Consequently, beam's kinematic hypothesis of linear strains is no longer valid. The predicted joint shear demand resulted underestimated by $\beta$-factor approach by 50%. Since 2D FEM may be not efficient for many practical circumstances, an application of Strut-and-Tie is alternatively proposed. Finally, both the limitations and possible extensions of the proposed approaches are stated transparently.

KEYWORDS

anchorage, beam–column joint, haunch retrofit, reinforced concrete, stress field analysis, Strut-and-Tie

## 1 | INTRODUCTION

Haunch retrofit solution dates back soon after Northridge (California) 1994 earthquake. In that case, damage to steel moment-resisting frames was extensive, indicating that the typical detail of welded flange-bolted web connection, used from the early 1970s, had inherent performance problems. The fracture of bottom flange weld was frequently reported[1] in the absence of inelastic beam deformations. Welding a triangular haunch beneath the beam's bottom flange significantly

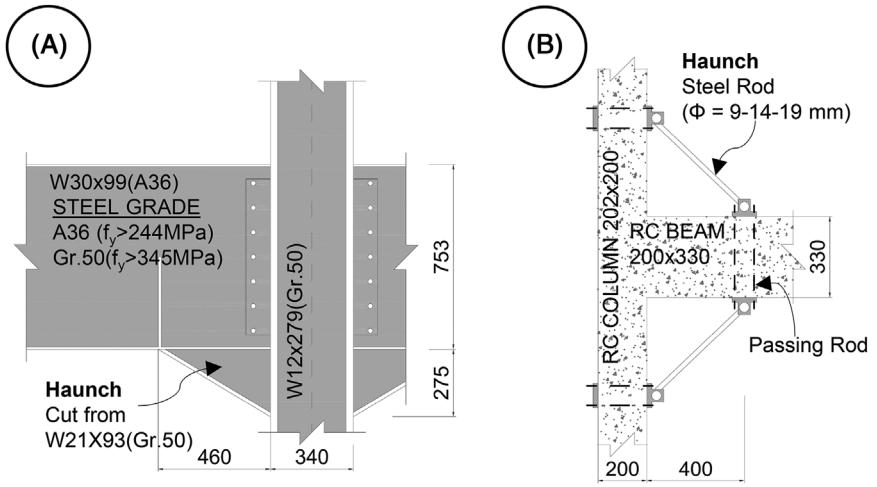


**FIGURE 1** Beam–column joints retrofitted using haunch: (A) steel prototype tested by Yu[2] ; (B) RC prototype tested by Pampanin[4]. (Notes. Dimensions are in millimeters.) RC, reinforced concrete.

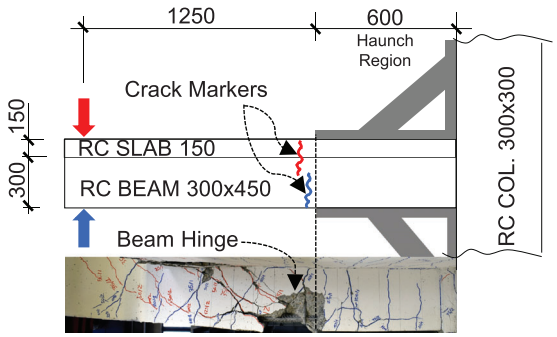


**FIGURE 2** Beam's crack pattern of an haunch retrofitted beam–column joint. (Notes. The specimen, represented in the picture, was tested[7] by the authors of this paper. Dimensions are in millimeters. The Reader is referred to the color version of this figure.).

improved the seismic performance of the connections as experimentally proven by Yu.[2] The tested prototype is shown in Figure 1A.

Application to reinforced concrete (RC) beam–column joints was subsequent and, to the Authors' knowledge, is due to Pampanin[3,4] and Chen[5] who first carried out an experimental campaign at the University of Canterbury. Their tested prototype is represented in Figure 1B.

For a RC joint, haunch lowers the joint shear demand with the intent of promoting ductile failure such as the beam's plastic hinge. Aside from the issue of invasiveness, which is undoubtedly impactful for retrofit of existing structures, haunch technology has a reduced cost if compared to fiber reinforced polymers, which is widely promoted nowadays.[6]

Typical crack pattern at failure of an RC beam–column joint, retrofitted with haunches is shown in Figure 2. The specimen was tested[7] by the authors of this paper. Mixed shear–flexural cracks developed outside the haunch region for both load directions. Plastic hinge formed in the beam, for sagging bending moment, at the boundary of the haunch-end. Moderate crack pattern characterized the haunch region. Occasionally inverted inclination of shear cracks has been observed[8] inside the haunch region. Such experimental observations suggest that bending moment should reduce in the haunch region whereas change of shear sign could happen.

The solution of internal forces for a beam–column joint retrofitted with haunch was primarily developed for steel structures[2] and then adapted to RC.[4] In particular, being the structure redundant, the compatibility of displacements between haunch and beam (or column) is assumed. Both the haunch region and the remaining beam segment are studied under linear-strains hypothesis, according to classical beam theory. Such approach will be referred as "$\beta$-factor approach" throughout this paper.

It is wondered whether extended haunches with stiff diagonals may violate the beam theory hypothesis. To prove it, stress field of the retrofitted joint is investigated by means of two-dimensional (2D) FEM models. Being such method not efficient for practical circumstances, an application of Strut-and-Tie method (STM) is proposed alternatively.

The plan of the paper is as follows: the state-of-the-art of haunch retrofit applied to RC beam–column joint is presented at Section 2. $\beta$-factor approach is critically discussed at Section 3. 2D FEM models, for selected benchmarks, are presented in Section 4. An application of STM, alternative to 2D FEM, is given at Section 5. Section 6 discusses the limitations of the results. Finally, Section 7 includes both a summary and the main findings of the presented research.

## 2 | BACKGROUND

This section presents a literature survey based on two major keyword, that is "RC beam–column joint" and "haunch retrofit." For the sake of clarity, the studies are reviewed by distinguishing the adopted investigation method, that is, experimental, analytical, or numerical.

### 2.1 | Experimental studies

A data collection obtained from reviewed experimental studies is presented in Table 1. The database includes 36 tests carried out on 2D exterior joints. Data of full-scale tests on portal frame[9] could not be directly used in the proposed meta-analysis. The table includes both retrofitted specimens and reference tests, that is specimen tested without retrofit having the same geometry, reinforcement layout, and nominal materials properties. All the specimens are characterized by absence (or low-percentage) of joint horizontal reinforcement. The flexural strength ratio ($\frac{\Sigma Mc}{\Sigma Mb}$) roughly ranges from 1.0 to 2.5 with out-of-range values due to adoption of shallow beams.[10,11] Low-to-medium concrete strength is usually assumed. The ratio between peak loads in the retrofit test and in the reference test (Ret-to-Ref) has been calculated considering (i) the case of highest peak for more than one reference test and (ii) different load direction for specimens with slab (positive assumes the slab in tension). Joint shear failure has been declared for all the reference tests, possibly with contemporary yielding of the beam longitudinal rebars. Ret-to-Ref ratio higher than 1 characterizes all the retrofitted specimens. Exceptions are represented by tests carried out with haunches installed after joint shear failure. Generally, retrofitted specimens failed with beam's plastic hinge, only few cases reported either anchor failure or haunch yielding. Figure 3 shows the possible influence of the design parameters on the Ret-to-Ref ratio. Double haunch configuration has been used by the majority of investigators, consequently the scatter obtained for Ret-to-Ref ratio is higher with respect to the single configuration. The haunch length to beam-span ratio ($L'/L_{beam}$) has values centered in 0.10 and nonspecific relationship with Ret-to-Ref ratio is observed. Haunch stiffness ranges almost over three order of magnitude, that is, from $10^4$ to $10^6$ N/mm. Increasing the haunch stiffness does not increase the Ret–to–Ref ratio. Such evidence is a consequence of limited redistribution, which should be expected from haunch installation. In fact, although retrofitted joint can be generally considered as redundant structure, load increment after the formation of plastic hinge in the beam cannot be sustained due to the formation of a kinematic mechanism.

### 2.2 | Analytical studies

Closed-form solution of beam–column joint retrofitted with haunches belongs to steel researchers community. Specifically, Yu[2] first defined the $\beta$-factor by presenting the solution of a steel cantilever with a single haunch. The analytical model has been included in AISC guideline[12] as a design method for seismic retrofit of MRF. Comparison with FEM was recently made by Zhao[13] who claimed that the analytical prediction of internal forces shows agreement in the elastic range but the connection capacity is underestimated in the post-yielding mainly because the model neglects redistribution, which happens both at the joint shear panel and at the haunch's flange. Extension of $\beta$-factor approach to RC beam–column joint is due to Pampanin.[3–5]. Comprehensive review has been made by Zabihi.[14] This paper critically addresses the $\beta$-factor application to RC at Section 3.

### 2.3 | Numerical studies

Numerical studies can be further subdivided on the basis of the targeted structural scale, that is, beam–column joint subassemblage or frame. In both cases, haunches are introduced in FEM models as beam elements connected both to

**TABLE 1** Database of experimentally tested RC beam–column joint retrofitted with haunch.

| Author notes – | Test – | $f_c$ (MPa) | $h_b$ (a) (mm) | $\rho_{s1}$ (b) (%) | $\rho_{sh}$ (c) (%) | $L'/h_b$ (d) (–) | $L'/L_b$ (e) (–) | $K_h$ (f) (⋆) | H (g) (–) | FR (h) (–) | $R-t-R$ (i) (–) | F (j) | $\beta$ (k) (–) | M.Red.F (l) (–) |
|---|---|---|---|---|---|---|---|---|---|---|---|---|---|---|
| Truong | *J*−0 | 21 | 300 | 2.4 | 0.0 | – | – | – | – | 2.27 | – | BY-JS | – | – |
| [31] | *J*−*H* | 20 | 300 | 2.4 | 0.0 | 1.4 | 0.09 | 225 | 1 | 2.27 | 1.46 | BY-HF | 4.65 | −0.34 |
| Genesio | *2Dpre* | 18 | 330 | 0.4 | 0.0 | – | – | – | – | 1.02 | – | JS | – | – |
| [29] | *JT1* | 25 | 400 | 0.7 | 0.0 | – | – | – | – | 2.45 | – | JS | – | – |
| and | *2DG1* | 17 | 330 | 0.4 | 0.0 | 1.1 | 0.11 | 119 | 2 | 1.02 | 0.84 | JS | 3.09 | −0.17 |
| Sharma | *2DG2* | 17 | 330 | 0.4 | 0.0 | 0.6 | 0.07 | 111 | 2 | 1.02 | 1.29 | BY-BF | 3.55 | 0.07 |
| [22] | *JT12* | 27 | 400 | 0.7 | 0.0 | 0.9 | 0.10 | 63 | 2 | 2.15 | 1.60 | BY-BF | 2.66 | 0.13 |
| | *JT13* | 30 | 400 | 0.7 | 0.0 | 0.9 | 0.10 | 63 | 2 | 2.15 | 1.57 | BY-BF | 2.63 | 0.14 |
| | *JT14* | 34 | 400 | 0.7 | 0.0 | 0.9 | 0.10 | 63 | 2 | 2.15 | 1.31 | BY-BF | 2.60 | 0.15 |
| | *JT15* | 28 | 400 | 0.7 | 0.0 | 0.9 | 0.10 | 63 | 2 | 2.15 | 1.05 | BY-BF | 2.65 | 0.13 |
| Sharbatdar | *SC1* | 16 | 150 | 0.9 | 0.3 | – | – | – | – | 5.97 | – | BY-JS | 0.00 | 0.00 |
| [10] | *SC2* | 16 | 150 | 0.9 | 0.3 | – | – | – | – | 5.97 | – | BY-JS | 0.00 | 0.00 |
| | *RSC1* | 16 | 150 | 0.9 | 0.3 | 2.0 | 0.11 | 8 | 2 | 5.97 | 1.33 | BY-HF | 3.08 | 0.10 |
| | *RSC2* | 16 | 150 | 0.9 | 0.3 | 2.0 | 0.11 | 8 | 2 | 5.97 | 1.92 | BY-HF | 3.08 | 0.10 |
| Pampanin | *TDP2* | 23 | 330 | 0.5 | 0.1 | – | – | – | – | 1.19 | – | JS | – | – |
| [4] | *THR1* | 26 | 330 | 0.5 | 0.1 | 1.2 | 0.13 | 6 | 2 | 1.03 | 1.54 | BY-BF | 1.20 | 0.74 |
| | *THR2* | 26 | 330 | 0.5 | 0.1 | 1.2 | 0.13 | 2 | 2 | 1.03 | 1.60 | BY-BF | 0.65 | 1.05 |
| | *THR3* | 27 | 330 | 0.5 | 0.1 | 1.2 | 0.13 | 11 | 2 | 1.03 | 1.57 | BY-BF | 1.66 | 0.48 |
| Marchisella | *S01+* | 24 | 450 | 1.0 | 0.0 | – | – | – | – | 1.46 | – | JS | – | – |
| [7] | *S01−* | 24 | 450 | 1.0 | 0.0 | – | – | – | – | 1.46 | – | JS | – | – |
| (†) | *S02+* | 23 | 450 | 1.0 | 0.0 | – | – | – | – | 1.46 | – | JS | – | – |
| | *S02−* | 23 | 450 | 1.0 | 0.0 | – | – | – | – | 1.46 | – | JS | – | – |
| | *S01R+* | 24 | 450 | 1.0 | 0.0 | 0.9 | 0.09 | 80 | 2 | 1.46 | 0.89 | JS | 3.15 | 0.04 |
| | *S01R−* | 24 | 450 | 1.0 | 0.0 | 0.9 | 0.09 | 80 | 2 | 1.46 | 1.03 | JS | 3.15 | 0.04 |
| | *S03+* | 36 | 450 | 1.0 | 0.0 | 0.9 | 0.09 | 80 | 2 | 1.46 | 1.54 | BY-HF | 3.05 | 0.08 |
| | *S03−* | 36 | 450 | 1.0 | 0.0 | 0.9 | 0.09 | 80 | 2 | 1.46 | 1.71 | BY-HF | 3.05 | 0.08 |
| | *S04+* | 31 | 450 | 1.0 | 0.0 | 0.9 | 0.09 | 80 | 2 | 1.46 | 1.92 | BY-BF | 3.08 | 0.07 |
| | *S04−* | 31 | 450 | 1.0 | 0.0 | 0.9 | 0.09 | 80 | 2 | 1.46 | 1.83 | BY-BF | 3.08 | 0.07 |
| Kheyroddin | *DSJ* | 16 | 150 | 0.9 | 0.3 | – | – | – | – | 5.97 | – | BY-JS | – | – |
| [11] | *RSJ1* | 15 | 150 | 0.9 | 0.3 | 2.0 | 0.10 | 5 | 1 | 5.97 | 1.52 | BY-HF | 3.05 | 0.23 |
| | *RSJ2* | 16 | 150 | 0.9 | 0.3 | 2.0 | 0.10 | 8 | 1 | 5.97 | 1.71 | BY-HF | 3.59 | 0.05 |
| | *RSJ3* | 15 | 150 | 0.9 | 0.3 | 2.0 | 0.10 | 15 | 1 | 5.97 | 1.69 | BY-HF | 4.09 | −0.12 |
| | *RSJ4* | 16 | 150 | 0.9 | 0.3 | 2.0 | 0.10 | 8 | 1 | 5.97 | 1.77 | BY-HF | 3.60 | 0.05 |
| Kanchanadevi | *SP1* | 41 | 400 | 0.7 | 0.0 | – | – | – | – | 1.89 | – | JS | – | – |
| [62] | *SP1H* | 39 | 400 | 0.7 | 0.0 | 1.0 | 0.13 | 21 | 1 | 1.89 | 1.28 | BY-BF | 1.30 | 0.61 |
| | *SP1BH* | 39 | 400 | 0.7 | 0.0 | 1.0 | 0.11 | 23 | 1 | 1.89 | 1.60 | BY-BF | 1.77 | 0.50 |

a,b,c,d,e,fConcrete cylindrical compressive strength ($f_c$); beam height ($h_b$); percentage of beam longitudinal reinforcement ($\rho_{sl} = max[\rho_{s1}; \rho_{s2}]$); percentage of joint horizontal reinforcement ($\rho_{sh}$); haunch length-to-beam depth ratio ($L'/h_b$); Haunch length-to-beam net span ratio ($L'/L_b$); haunch stiffness ($K_h$) dimension is (N/mm·$10^4$) (⋆).

gHaunch configuration: [-]Reference test; [1] single haunch; [2] double haunch.

hFlexural ratio, that is, $\frac{\Sigma Mc}{\Sigma Mb}$.

iRetrofit-to-reference peak load ratio.

jModes of failure: [BY] Beam yielding; [BF] beam flexural failure; [HF] anchorage or haunch failure; [JS] joint shear failure.

k$\beta$-factor evaluated according to Equation 2.

lM.Red.F. evaluated according to Equation 5.

†Suffixes to the test code indicate hogging (+) and sagging (-) behavior of the beam.

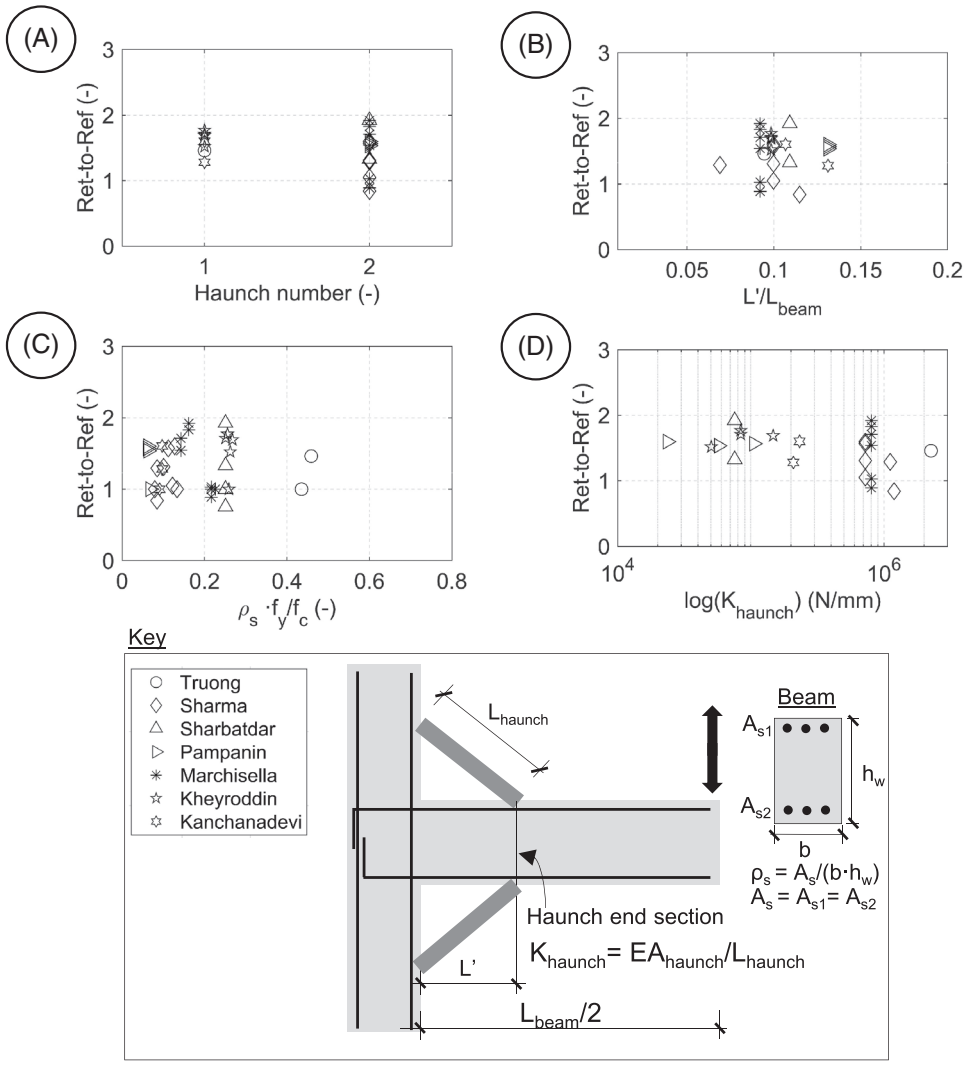


**FIGURE 3** Influence of design parameters on the Retrofit-to-Reference (R-t-R) strength ratio for the database of beam–column joints retrofitted with haunch: (A) haunch number; (B) haunch horizontal length to beam-span ratio; (C) mechanical reinforcement ratio of beam longitudinal bar; (D) haunch stiffness.

the beam and the column via rigid links.[9,15,16] Sharma[17] claimed that the connection should employ nonlinear springs, which load capacity and stiffness must be evaluated in different load–displacement stages. Zabihi[14] conducted a parametric study at the subassemblage scale, by varying (i) single or double haunch installation, (ii) the length of haunch diagonal and, (iii) beam–column span-to-length ratio. Strength hierarchy method[18] was used to determine the failure mode. Generally, haunch retrofit promoted beam hinging with respect to joint shear failure. Besides, for the same amount of haunch material being utilized in single or double configuration of the haunch, greater enhancement was obtained by implementing the latter. At the frame scale, MRF conceived without seismic details are usually employed as prototypes. For example, Ahmad[19] considered the results of pushover analysis carried out on two-dimensional MRF. Comparing the capacity curves for deficient and retrofitted frames, it was observed that the retrofit resulted in an increased lateral stiffness by 84% and maximum strength by 36%. By using similar two-dimensional MRF but investigating the response via NLTH, Akbar[20] found an average value of the response-modification factor[21] equal to 7.5. Sharma[22] studied a low-rise three-dimensional MRF by using NLTH response. Beam–column joint was modeled using multispring approach.[17,23,24] Haunches were applied only to the joints which displayed joint shear failures in the as-built condition. The retrofitted MRF was able to develop beam hinging with no major shear failure. Hysteretic responses of the joints remained in the elastic regime. Column hinges were formed at the base and minor damage was observed at the storey level. Shear demand for beams and columns was not critical neither for as-built condition nor for retrofitted one.

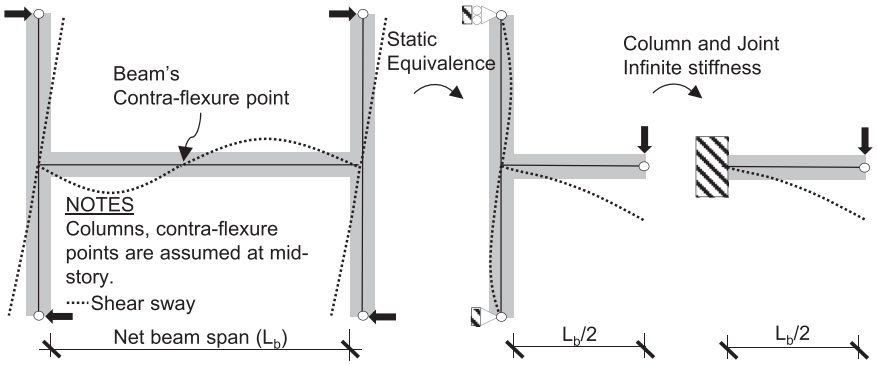


**FIGURE 4** Definition of beam–column joint subassemblage for a one bay half-story frame under shear sway.

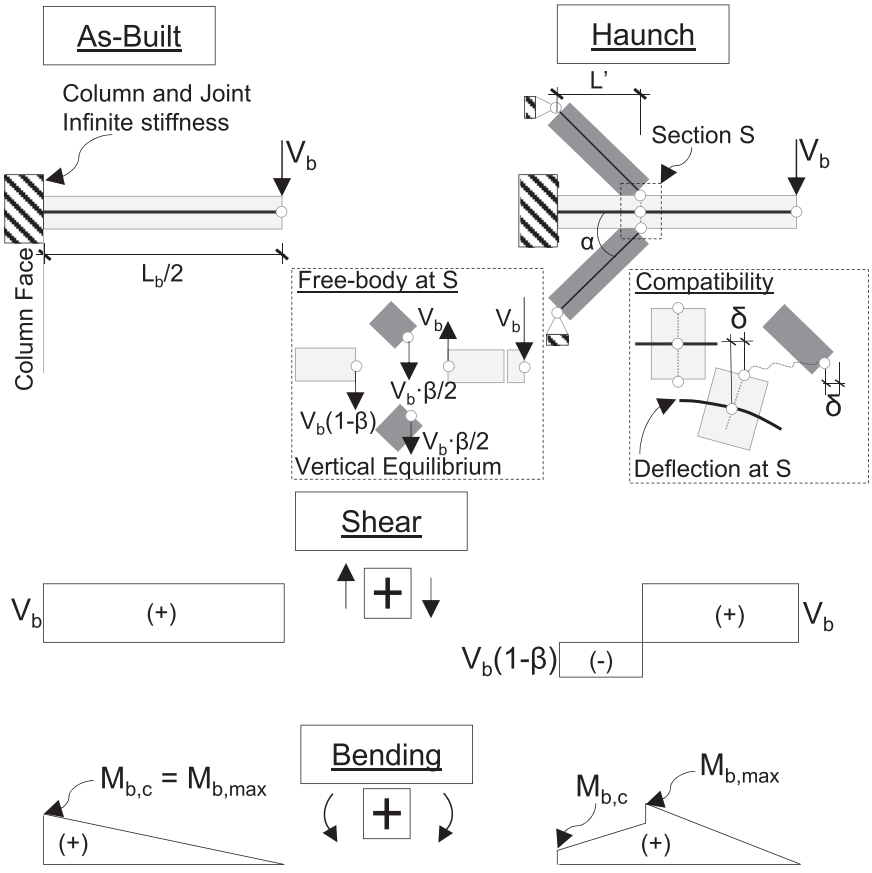


**FIGURE 5** Structural analysis of a cantilever retrofitted with double haunch.

## 3 | REVIEW OF THE $\beta$-FACTOR MODEL

### 3.1 | Original formulation

Consider the beam–column joint subassemblage definition represented in Figure 4. As commonly adopted[25,26] for MRF under shear-sway, contraflexure points are located in the middle of beams' spans and interstorey height. If both the column's and joint's stiffness are assumed infinite, the cantilever scheme applies to the beam. Figure 5 shows shear and bending moment diagrams under the application of tip load ($V_b$) downward. The as-built condition is statically determinate, characterized by linear and constant diagram for bending moment and shear, respectively. Haunches (either single or double configuration) turn the structure redundant, although the reactions at restraints remain statically determinate. According to Pampanin,[4] internal forces are obtained by imposing the compatibility of the haunch displacement at section $S$. The shear portion taken by the haunches is equal to $\beta V_b$ where $\beta$-factor is larger or equal than zero. As a result, the beam's shear diagram has a discontinuity. The maximum bending moment ($M_{b,max}$) is attained at section $S$, while it

decreases linearly till the column face to a value $M_{b,c}$ according to the following relationship:

$$M_{b,c} = M_{b,max}\left[1 - \frac{\beta d_b}{2Ltan\alpha} + \frac{(1-\beta)L'}{L_b/2 - L'}\right] \tag{1}$$

where $L_b$ is the beam span, $L'$ is the haunch horizontal length, $\alpha$ is the angle between the haunch diagonal and the horizontal direction. $\beta$ is defined as it follows:

$$\beta = \frac{b}{a} \cdot \frac{6Ld_b + 3ad_b + 6bL + 4ab}{3d_b^2 + 6bd_b + 4b^2 + (12EJ_b/2K_d a\cos(\alpha))} \tag{2}$$

where $a = L'$, $b = L'\tan(\alpha)$, $EJ_b$ is the beam flexural modulus, $d_b$ is the beam depth, $K_h = E_d A_d / L_d$ the axial stiffness of the haunch. Apart from double haunch stiffness contribution, Equation (2) is identical to what was derived by Yu[2] for steel cantilever. Nevertheless, Pampanin[4] formulated two additional definitions of $\beta$-factor by relaxing the infinite stiffness either of column or joint. For the sake of synthesis, they are not reported here. Generally, $\beta$-factor tend to be lower up to 15%–20% if the sole beam flexibility is considered. Pampanin[4] compared the closed-form solution with respect to FEM analysis assuming linear-elastic beam elements. The presentation of the FEM models lacked in details such as: (i) the definition of master-slave constraint to account for the eccentricities (e.g., $\pm d_b/2$) with respect to the beam axis; (ii) the definition of moment release for the haunch; (iii) the definition of flexural stiffness reduction (due to cracking[27]) possibly different for the beam and the column being the latter generally characterized by reduced damage due to the presence of axial load. As per the last issue, Emami[28] proposed to consider the cracked inertia both for the column and beam. Considering the bending moment at column face, one might expect that larger value of $\beta$-factor are desirable to reduce the horizontal shear transferred to the joint panel, as it is discussed subsequently in this paper. However, Pampanin suggested to assume value of $\beta$-factor less than 2 to avoid an excessive increase of shear demand for both the beam and column. Genesio[29] considered different values of the $\beta$-factor coming either from compressed or tensioned haunch. In fact, reduced stiffness is expected from the latter because of the anchorages pullout. Conversely, hard contact between the steel plates and concrete in a compressed haunch promotes stiffness increase. Emami[28] concluded that two are the decisive design parameter for haunch retrofit, that is, $L'/L_b$ and $K_h$. A simplified procedure to get the optimum $\beta$-factor was proposed by using linear regression. $L'/L_b$ was assumed equal to 0.15 and $\alpha$ equal to 45°. In this instance, the reduction of joint shear demand between as-built and retrofit joint ($V_{jh,haunch}/V_{jh}$) can be expressed as

$$\frac{V_{jh,haunch}}{V_{jh}} = -0.27ln(\lambda) + 0.24 \tag{3}$$

where

$$\lambda = \frac{E_d}{E_c}\frac{A_h}{I_b}\frac{L_b}{L'}cos(\alpha) \tag{4}$$

To summarize, the internal forces of a beam–column joint retrofitted with haunches can be defined as a function of the $\beta$-factor. For example, $\beta/2V_b$ is the vertical component of the haunch's diagonal force. Formulas, which relate the internal forces to design variables (e.g., $L', \alpha, K_h$), are nonlinear as much as their trend should be studied with multiple parametrical analyses, as it is shown in the following.

## 3.2 | Benchmarks

$\beta$-factor has been experimentally validated by Pampanin[4] by comparing analytical predictions with respect to experimentally derived values. For the latter, there was not a clear statement of the derivation's assumptions. In all likelihood $\beta$-factor was back-evaluated from haunch's diagonal displacement, being this measured via linear displacement transducers during test. Table 2 presents the evaluated $\beta$-factors for specimens tested by Pampanin.[4] Additionally, specimen tested by Genesio[29] is considered as well. Results obtained using Equation (2) are compared to the values retrieved from the original publications. Although the results are comparable, differences between $\beta$-factor values evaluated according to

**TABLE 2** Result of $\beta$-factor calculated for selected benchmarks.

| Specimen | Ref. | $\Phi$ (mm) | $L_h$ (mm) | $K_h$ (kN/m) | $\beta_{th.}$ (-) | $\beta_{exp}$ (-) | $A$ (mm$^2$) | $K_h$ (kN/m) | $\beta$ (-) |
|---|---|---|---|---|---|---|---|---|---|
| | | † | † | † | † | † | † | ∗ | ⋆ |
| THR1○ | [4] | 14 | 565 | 25,000 | 1.15 | 1.20 | 154 | 54,464 | 1.20 |
| THR2○ | [4] | 9 | 565 | 22,000 | 1.07 | 1.10 | 64 | 22,508 | 0.65 |
| THR3○ | [4] | 19 | 565 | 111,000 | 2.17 | 2.00 | 283 | 100,313 | 1.66 |
| JT1-4⊓ | [29] | - | 800 | 600,000 | 2.06 | - | 2400 | 600,000 | 2.60 |

○ Circular section. The area is evaluated as $A_h = 0.25\Phi^2\pi$.
⊓ Rectangular section 16 × 150 mm.
† Retrieved from original publications [4,29].
∗ Evaluated as $E_s A_h / L_h$, assuming $Es$ equal to 200 GPa.
⋆ Evaluated by applying Equation (2).

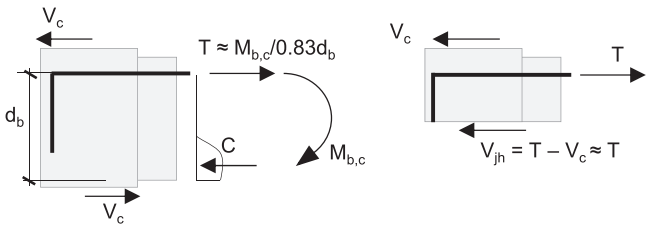


**FIGURE 6** Definition of the horizontal joint shear demand ($V\_jh$) for an exterior RC beam.column joint. RC, reinforced concrete.

Equation (2) and original ones are most probably due to the neglection of column's deformability assumed by the former. The following Section 4 of this paper considers specimens THR1 and JT1-4 as benchmarks. It is worth to mention that for these two cases, differences between Equation (2) and original values are 4 and 26%.

## 3.3 | Parametric study

The parametric study presented in the following assumes as relevant design parameter the moment reduction factor (M.Red.F) derived from Equation (1) as it follows:

$$M.red.F = \frac{M_{b,c}}{M_{b,max}} = 1 - \frac{\beta d_b}{2Ltan\alpha} + \frac{(1-\beta)L'}{L_b/2 - L'} \tag{5}$$

Such output is crucial for the evaluation of haunch retrofit performance. In fact, by assuming $M_{b,max}$ equal to the yielding capacity of the beam, the M.Red.F can be assimilated to the reduction of joint shear demand between as-built and retrofitted joint. In fact, as can be inferred from Figure 6, the horizontal joint shear demand ($V_{jh}$) is linearly dependent on $M_{b,c}$ according to the following relationship:

$$V_{jh} = \frac{M_{b,c}}{0.83d_b} - V_c \approx \frac{M_{b,c}}{0.83d_b} \tag{6}$$

where the contribution of the column's shear ($V_c$) to the horizontal equilibrium can be neglected because the ratio $V_{jh}/V_c$ amounts to a value between four to six[30] in an as-built joint. For the sake of simplicity, same assumption is made for a retrofitted joint, although $V_c$ may change sign in the Equation (6) depending on $\beta$-factor. On this subject, a further discussion is presented in Section 4.

To study the impact of the design variables affecting the M.Red.F, an artificial dataset is generated. The considered structure is a "double haunch cantilever" with a downward force applied at the beam tip. The considered parameters, and their ranges, are listed as it follows:

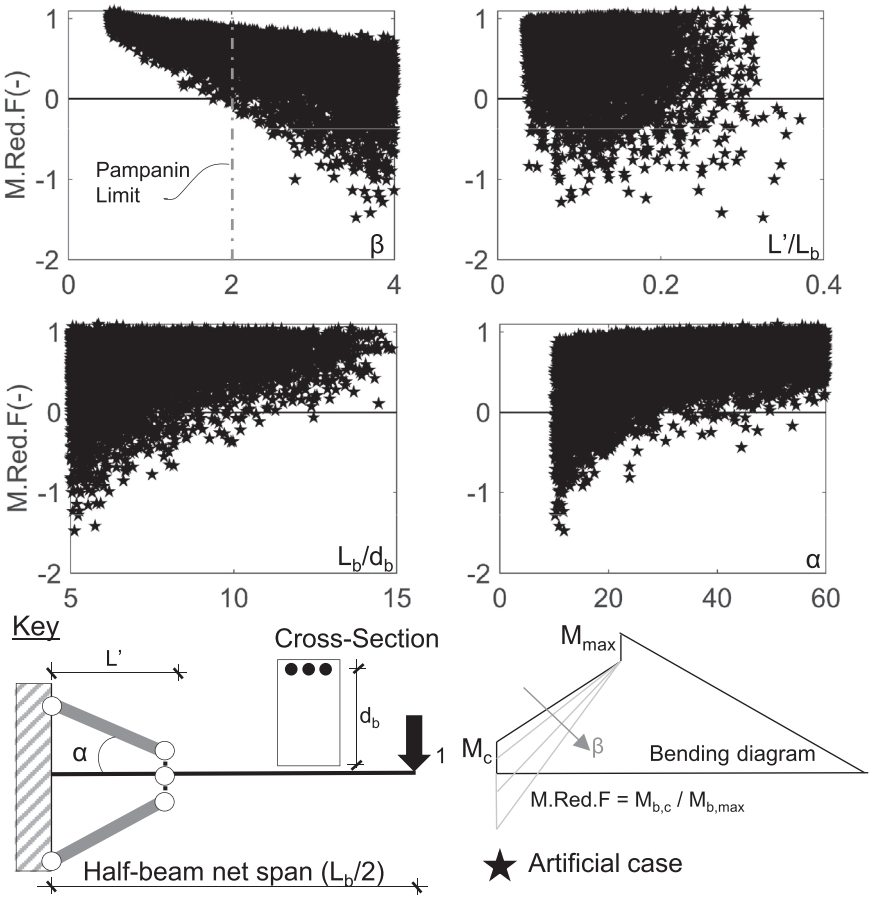


**FIGURE 7** Effect of design variables on the moment reduction factor (M.Red.F) in a cantilever with two haunches.

- $\beta$-factor. From 0.5 to 4.0.
- $L_b$. From 2.0 to 6.0 m.
- $L'$. From 20 to 300 cm.
- $d_b$. From 20 to 80 cm.
- $\alpha$. From 10° to 60°.

The obtained M.Red.F are represented in the Figure 7 as a function of the design variables. Values of $\beta$-factor larger than two (limit defined by Pampanin[4] to avoid excessive shear either in the beam or in the column) lead to M.Red.F zero or even lower than zero. The same trend is observed either when decreasing the beam aspect ratio ($L/h_b$) or when increasing $L'$. According to Equation (5), M.Red.F less than zero should imply an inversion of moment sign at column face. Besides, according to Equation (6), horizontal joint shear demand should change sign as well. Such inversion, to the authors' knowledge, has no experimental evidence. For example, specimen "J-H" tested by Troung[31] is characterized by M.Red.F less than zero according to Table 1. However, neither the sign inversion of experimentally derived rebars' strains at column face nor inverted cracks at the joint panel were reported. Generally, $\beta$-factor approach may differ from the actual mechanical response of a RC retrofitted joint because the assumed compatibility condition between haunch and beam (or column) may be inconsistent. In this regard, the joint's stress field has been studied by using 2D FEM, as it is presented in the following.

## 4 | FINITE ELEMENT MODELS

### 4.1 | Models details

Specimens JT1-4 and THR1, tested by Genesio[29] and Pampanin,[4] respectively, are considered in the presented numerical investigation. The specimens were selected to investigate how different haunch's geometry (e.g., cross-section of the

**TABLE 3** Data of benchmark specimens JT1-4 and THR1, tested by Genesio [63] and Pampanin [4].

| | | JT1-4 | THR-1 |
|---|---|---|---|
| *Geometry* | | | |
| $L_b/2$ | (mm) | 1750 | 1525 |
| $H_c$ | (mm) | 3200 | 2000 |
| $d_b$ | (mm) | 400 | 330 |
| $b_w$ | (mm) | 300 | 200 |
| $h_c$ | (mm) | 300 | 230 |
| $L'$ | (mm) | 600 | 400 |
| *Materials* | | | |
| $f_c$ | (MPa) | 33.6 | 25.9 |
| $f_{ct}$ | (MPa) | 3.1 | 2.6 |
| $f_y$ | (MPa) | 490 | 344 |
| *Joint cracking load*[a] | | | |
| $\nu$ | (-) | 0.00 | 0.05 |
| $V_{jh,cr}$ | (kN) | 279 | 150 |
| *Beam flexural properties*[b] | | | |
| $M_{cr}$ | (kNm) | 24.8 | 9.5 |
| $M_y$ | (kNm) | 93.6 | 28.2 |
| *Beam shear properties*[c] | | | |
| $V_{R,c}$ | (kN) | 34.6 | 20.5 |
| $V_{R,s}$ | (kN) | 86.2 | 66.7 |
| *Beam load*[d] | | | |
| $V_b$ | (kN) | 90 | 30 |
| *β-factor* | | | |
| $\beta$ | (-) | 2.60 | 1.20 |
| $M_{b,c}/M_{b,max}$ | (-) | 0.15 | 0.75 |

[a] $V_{jh,cr}$ is evaluated [51] as $V_{jh,cr} = A_j \cdot f_{ct}\sqrt{1+\nu f_c/f_{ct}}$, where $Aj$ is the joint area projected in the horizontal plane, $\nu$ is the normalized axial force in the column.
[b] $M_{cr}$ is the cracking moment, that is, $M_{cr} = f_{ct}b_w d_b^2/6$. $M_y$ is the yielding moment evaluated via sectional analysis using software Response2000 [64].A reduced steel area, with respect to nominal data, was assumed for JT1-4 because one bar was cut to weak the specimen.
[c] $V_c$ and $V_s$ are the shear resistances, according to ACI [32] for concrete and steel, respectively.
[d] Selected load stage to compare numerical results. Beam hogging behavior is studied.

diagonal, anchorage to concrete, extension of the base plate) may affect the joint's stress field. Specimens' data are available both at Tables 1 and 3. The experimentally derived envelopes of load–displacement curves are shown in Figure 8. As-built specimens were characterized by joint shear failure whereas retrofitted ones failed developing beam's plastic hinge. In the following, the numerical results are discussed with emphasis on both beam's flexural response and joint shear demand. Although the authors are aware that shear force induced in beam (or column) may be an issue in many practical assessment cases, this is not discussed for a twofold reason: (i) experimental results did not report shear weakness neither for the beams nor for the columns; (ii) the nominal shear resistances, evaluated as summation of concrete and steel contribution according to ACI guideline,[32] were proven to be enough larger with respect to numerically derived shear forces. Figures 9 and 10 show specimens' geometry as well as the boundary conditions used in the numerical models. Post-installed anchors and elongated base plate were used in JT1–4 whereas THR1 had reduced bearing plates and passing rods. Details of haunch diagonal cross sections were given in Table 2. For both the specimens, plane stress conditions was adopted for concrete and steel with the exception of THR1 where beam element was used for the haunch diagonal. Four-node quadrilateral elements, with the addition of four incompatible modes (Q6 element[33]), were used with mesh size equal to 20 mm. The mesh was structured, that is, all the element were undistorted. Linear-elastic constitutive laws were assumed both for concrete and steel. Reinforcement bars were not modeled explicitly. The load was applied to the beam tip. Anchorages to concrete of specimen JT1-4 were modeled using beam elements connected to the surrounding concrete via bond springs. The relative displacement between the connected nodes of the spring represents the slip between the anchor and concrete, whereas the nodal spring force is the work equivalent of bond stresses

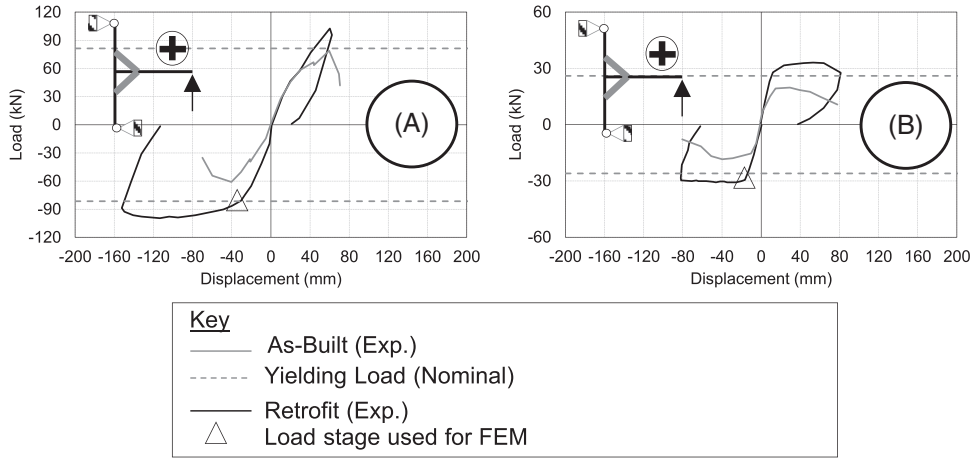


**FIGURE 8** Experimentally -derived load -versus -displacement envelopes of cyclically tested specimens: (A) tests carried out by Genesio2[29]; (B) tests carried out by Pampanin[4]. (Notes. Experimental data were digitally -derived, from the original publications, using GetData Graph Digitizer software. The prediction of beam yielding load, for retrofitted specimens, is computed using mean values for material parameters.).

**FIGURE 9** Finite element idealization of specimen "JT1-4" tested by Genesio[29]: (A) model layout; (B) anchors' modeling detail. (Notes. Dimensions are in millimeters. The Reader is referred to the color version of this figure).

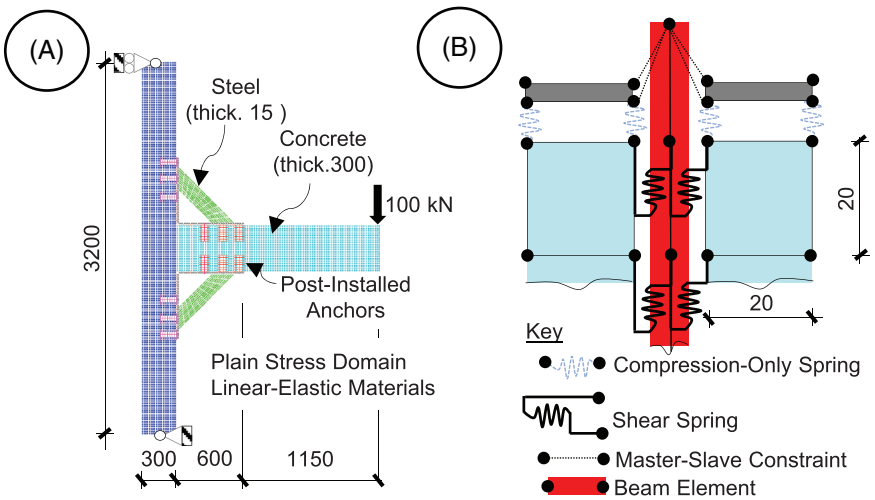


**FIGURE 10** Finite element idealization of specimen "THR1" tested by Pampanin[4]: (A) model layout; (B) passing rod modeling detail. (Notes. Dimensions are in millimeters. The Reader is referred to the color version of this figure.).

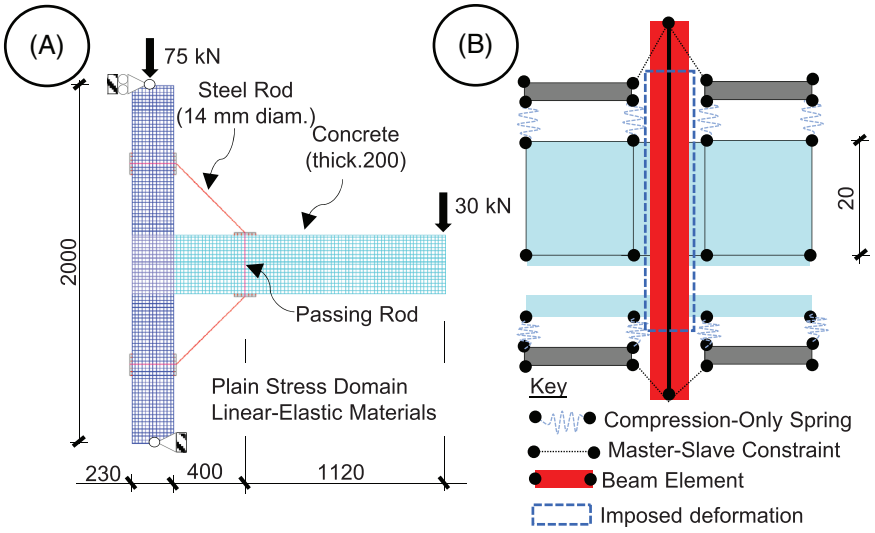

developed over the effective length of the beam elements adjacent to the node under consideration. The Model Code 2010[34] bond–slip law was assumed. In particular, the stiffness was evaluated as the secant of the first branch where (i) the peak bond stress was equal to 9 MPa and (ii) slip had a nominal value of 1 mm. The resulting anchors' stiffness was equal to almost 30% of the rod's elastic stiffness, that is, $E_s A_{rod}/L_{rod}$. Anchor prestressing was applied only for specimen THR1 by imposing a constant compressive strain equal to 3000 microstrains. Haunch plates were connected to concrete base with compression-only springs. The shear transfer, possibly mobilized by friction, was neglected. As a result, the anchors behaved as shear keys. Such assumption has been made (i) to reduce the number of degree of freedom and (ii) to prevent numerical instability deriving from the definition of springs with coupled stiffness. Both the anchors and the passing rods were connected to the plate holes via kinematic constraints. The selected load stage, for specimen JT1-4, is 90 kN applied downward at beam tip as marked in Figure 8A, which corresponded to almost 40 mm of imposed displacement during test. At this stage, the reinforcement strains were below the nominal yielding threshold. Under this circumstance, both concrete and steel were expected to behave linearly within the haunch region, thus the stress field predicted by linear-elastic analysis was supposed to be comparable. Same considerations were applied to specimen THR1 although results of the experimental strains were not available. Numerical analyses were performed using a commercial FEM software, that is, SAP2000.[35] Because of the adopted compression-only concrete bedding, the analysis was nonlinear, performed with load control.

## 4.2 | Results

### 4.2.1 | Specimens JT1 and JT1-4

Figure 11B shows the comparison between the compressive stress fields for JT1 (as-built) and JT1-4. Stresses were recovered at nodes after smoothing[36] the values at Gauss points ($2 \times 2$ grid). The magnitude of principal stresses reduces within the joint panel if JT1-4 is compared with JT1, confirming the expected reduction of the shear demand. Evidently, a main diagonal strut mechanism, which is qualitatively represented by dashed line in Figure 11C, dominates the response of JT1 joint panel. Nonetheless, a beam-type stress field (B-region) results in the remaining beam portion. Such stress flow, under hogging behavior, is characterized by horizontal tensile stresses at top and compressive at the bottom. As per the retrofitted condition, the stress compressive trajectories deviate from the joint panel to the haunch region due to the bearing mechanism promoted by the compressed haunch. As a result, the entire haunch region should be more properly defined as a D-region, where "D" stands for discontinuity.[37] To prove the inapplicability of beam theory, it is worth to derive the beam's curvature as it is shown in Figure 12. Starting from nodal values of deflection, the mean value between top, bottom edge and center-line is evaluated. Subsequently, the curvature is obtained by incrementally derive twice. The length increment coincides with the element size (i.e., 20 mm). The numerically derived curvatures are compared with closed-form solution of a cantilever having the span equal to the beam's net length both for JT1 and JT1-4. Specifically, the curvature is obtained dividing the bending moment by the flexural modulus. As a result, linear straight diagram characterizes JT1 (Figure 12B) whereas, for JT1-4, the diagram is bilinear (Figure 12C). As expected, numerical values agree with analytical prediction only in the B-regions where linear trend is clearly recognized. Conversely, curvature deviates from liner envelop both at the haunch region and at the beam's loaded end. Comparison of stress profiles, at relevant beam's cross-sections, is shown in Figure 14. $\beta$-factor approach assumes linear stresses along the beam height and constant stress profile for the haunch diagonal. At column face, the numerically derived stresses have a nonlinear distribution characterized by large gradients at the section edges. Neutral axis locates at the half depth of the cross-section. As per the haunch diagonal, a stress gradient is recognized. Such evidence might be due to the eccentricity of the anchors' resultant force. Nevertheless, larger diagonal force is obtained numerically with respect to experimental one because the anchors might have suffered larger slip than the one assumed by numerical models. All the numerically derived internal forces are presented in Table 4 and discussed in the following. Shear forces and bending moments at different beam's cross-sections were derived by integrating the numerical stresses with trapezoidal rule. Numerically derived bending moments are higher than the ones predicted by $\beta$-factor, the highest difference is found at the column-face section. The obtained values fall in the range between the nominal cracking moment and the yielding one. Numerically derived shear forces decrease from column face to haunch end. Values are similar to those predicted by the $\beta$-factor. Moreover, the two methods agree on the shear's sign change passing from haunch's region to outside. Aside from the differences between the predicted haunch forces and the experimental values, which was explained as a possible consequence of excessive slip of anchorages

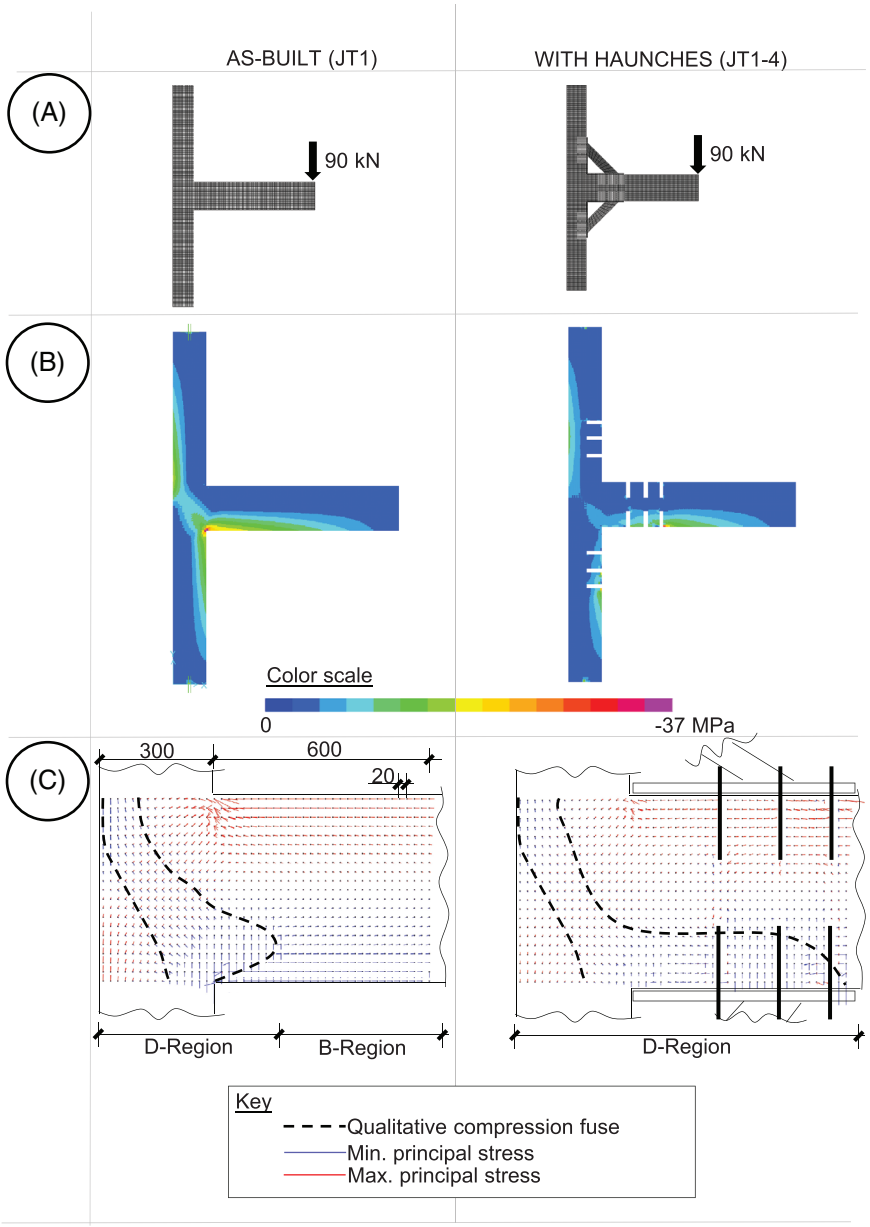


**FIGURE 11** Numerical results of specimens JT1 (left) and JT1-4 (right) tested by Genesio[29]: (A) models; (B) minimum principal stress plot; (C) stress trajectories inside the haunch region. (Notes. Dimensions are in millimeters. The Reader is referred to the color version of this figure.).

during the test, it is worth to mention that different numerically derived forces are obtained for compressed haunch and tensioned one. Such outcome has a twofold explanation: on one hand, different boundary conditions were applied at the top (lateral restraint) and bottom (lateral and vertical restraint) column's section, respectively; on the other, differences are expected from anchors' slip. An insight of the joint panel stress field is presented in Figure 13. By definition, the horizontal shear demand ($V_{jh}$) is the resultant of tangential stresses acting at the half-depth of a joint panel. The horizontal equilibrium is restored both by the column's shear ($V_c$) and the resultant of normal stresses ($T$) acting in the beam's half-depth. A small error affect the equilibrium equivalence mainly due to lack of accuracy of stress recovery at nodal points.[38] Nevertheless, it is noted that haunches caused a sign change of column's shear, which concurs to increase the joint shear demand unlike the as-built case. Numerically derived value of joint shear demand is more than two times the one obtained by adopting the $\beta$-factor approach, as can be inferred from Table 4. In the light of practical assessment, it is worth to mention that although the estimated shear demand does not overcame the nominal resistance, the safety margin that could have been obtained using $\beta$-factor approach is unconservative.

To validate the numerical models, experimental strains are retrieved for specimen JT1-4 from the original publication. The beam's top longitudinal reinforcement was instrumented with strain gauges at three different cross-section within

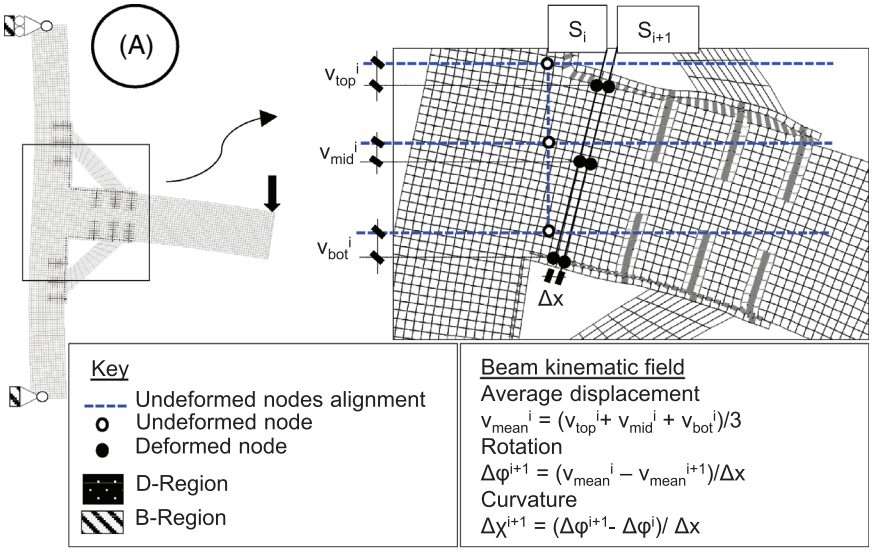


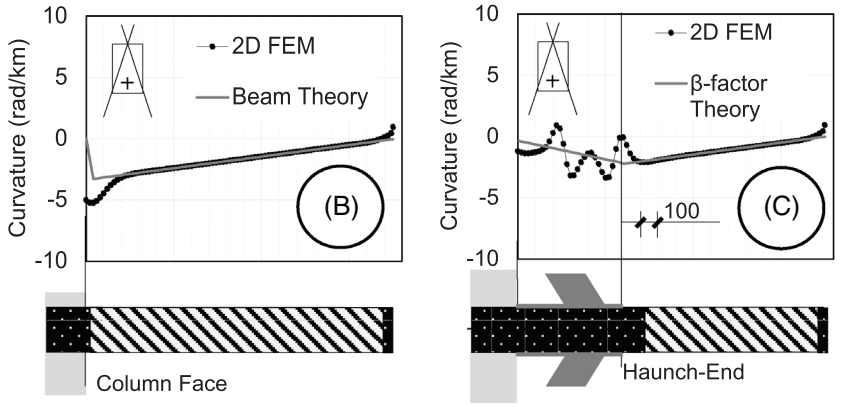


**FIGURE 12** Numerically -derived curvatures: (A) definition of beam's displacement field derived from nodal values; curvature diagrams for specimens JT1 (B) and JT1-4 (C) tested by Genesio[29]. (Notes. Dimensions are in millimeters. Displacements in the figure have been arbitrarily magnified for representation purposes. The Reader is referred to the color version of this figure.).

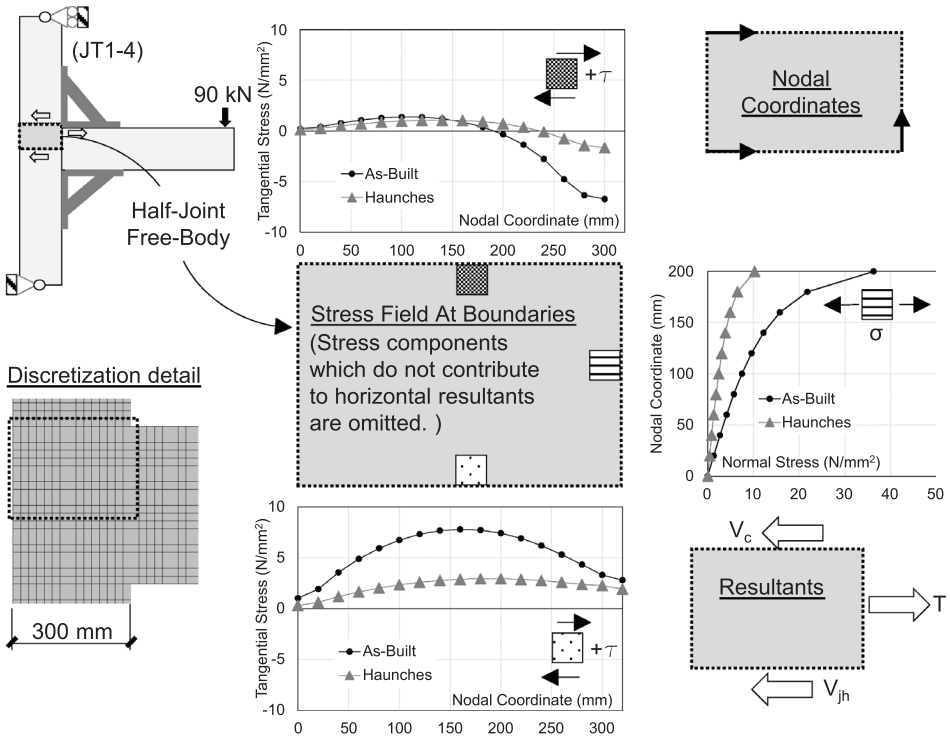


**FIGURE 13** Numerically -derived stress field at joint panel of specimen JT1-4, tested by Genesio[29].

**TABLE 4** Internal forces of specimen JT1-4, tested by Genesio [29].

| ***Beam***[b] | | 2D FEM[a] | | | β-factor | | | Exp. | STM |
|---|---|---|---|---|---|---|---|---|---|
| | $l_s$[c] (mm) | M (kNm) | V (kN) | $\epsilon_s$ ($\cdot 10^{-6}$) | M (kNm) | V (kN) | $\epsilon_s$ ($\cdot 10^{-6}$) | $\epsilon_s$[g] ($\cdot 10^{-6}$) | $\epsilon_s$ ($\cdot 10^{-6}$) |
| Column face | 0 | 36.7 | −144.1 | 643 | 15.5 | −144.0 | 271 | 624 | 1022 |
| Intermediate | 100 | 49.9 | −120.3 | – | 29.9 | −144.0 | – | – | – |
| Intermediate | 200 | 56.8 | −116.7 | – | 44.3 | −144.0 | – | - | – |
| Intermediate | 300 | 69.1 | −107.4 | 1211 | 58.7 | −144.0 | 1029 | 1129 | 1505 |
| Haunch end | 600 | 106.3 | 90.0 | 1864 | 103.5 | 90.0 | 1814 | 1962 | 2154 |
| Clear beam | 800 | 85.9 | 90.0 | 1506 | 85.5 | 90.0 | 1499 | 1049 | 1465 |
| ***Haunches*** | | | | | | | | | |
| | | $N^h$ | | | $N^h$ | | | $N^{hf}$ | $N^{hf}$ |
| | | (kN) | | | (kN) | | | (kN) | (kN) |
| (Tension) | | 124.8 | | | 165.5 | | | 78.0 | 78.0 |
| (Compression) | | 137.3 | | | 165.5 | | | 81.0 | 81.0 |
| ***Joint panel***[d] | | | | | | | | | |
| | | | | | | | | Nom.[h] | |
| $V_c$ | (kN) | −26.3 | | | −29.1 | | | – | – |
| $T$ | (kN) | 165.2 | | | 57.9 | | | – | – |
| $V_{jh} = T - V_c$ | (kN) | 191.5 | | | 87.0 | | | 279.0 | – |
| $V_{jh}^{num.(e)}$ | (kN) | 203.2 | | | – | | | – | – |

[a]Numerically derived internal forces are computed as integral of the stresses distributions.
[b]Hogging moments ($M$) are assumed positive. Clockwise shear forces ($V$) are assumed positive. $\epsilon_s$ is the strain at the top longitudinal reinforcement. Both the numerical value and $\beta$-factor values of $\epsilon_s$ are obtained by performing linear sectional analysis assuming $M$ as acting moment.
[c]Distance of the beam's cross-section from the column face.
[d]The sign convention of the horizontal forces acting at the joint panel is shown in Figure 13.
[e]$V_{jh}^{num}$ is numerically derived as the integral of tangential stresses acting at the half-joint depth.
[f]Haunch load was obtained from original publication where the values were back-derived from strain gauges glued onto the haunch diagonal.
[g]Experimental data of strain gauges readings were digitally derived, from the original publication, using GetData Graph Digitizer software.
[h]Nominal joint cracking resistance.

the haunch region and one outside. Although the beam was weakened by cutting one bar (16-mm diameter) at a distance of 50 mm from the haunch end, all the bars have been considered activated in the haunch region. In fact, at the column face, the bond length amounts to almost 20 times the diameter without considering the beneficial effect of bent anchorage. Numerically derived strains are obtained by post-processing 2D FEM results according to Figure 15. Specifically, bending moment was derived from 2D FEM, which assume uncracked concrete, then a sectional analysis followed by adopting the"transformed cracked cross-section."[39] Similar procedure was adopted for $\beta$-factor. Strain diagrams are shown in Figures 16 and 17. Additionally, the values are reported in Table 4. For the sake of synthesis, STM's values are included as well but they are discussed in Section 5 of this paper. Numerically derived strain is comparable to the experimental one at column face. $\beta$-factor predictions are generally lower.

### 4.2.2 | Specimen THR1

Numerical results obtained for specimen THR1 are presented in Figure 17 and Table 5. Generally, the haunch region proved to be less disturbed with respect to specimen JT1-4, previously discussed. However, deviations of stress trajectories are evident in the proximity of haunches' bearing plates. Differently with respect to specimen JT1-4, $\beta$-factor approach fairly agrees with numerically derived curvature within the haunch length. Consequently, agreement is found for the predicted internal forces. In this regard, sufficient accuracy might be expected from $\beta$-factor predictions for small haunch diagonal cross-section and bearing plate not extending till the column face. In fact, under such conditions, a B-region can still be identified.

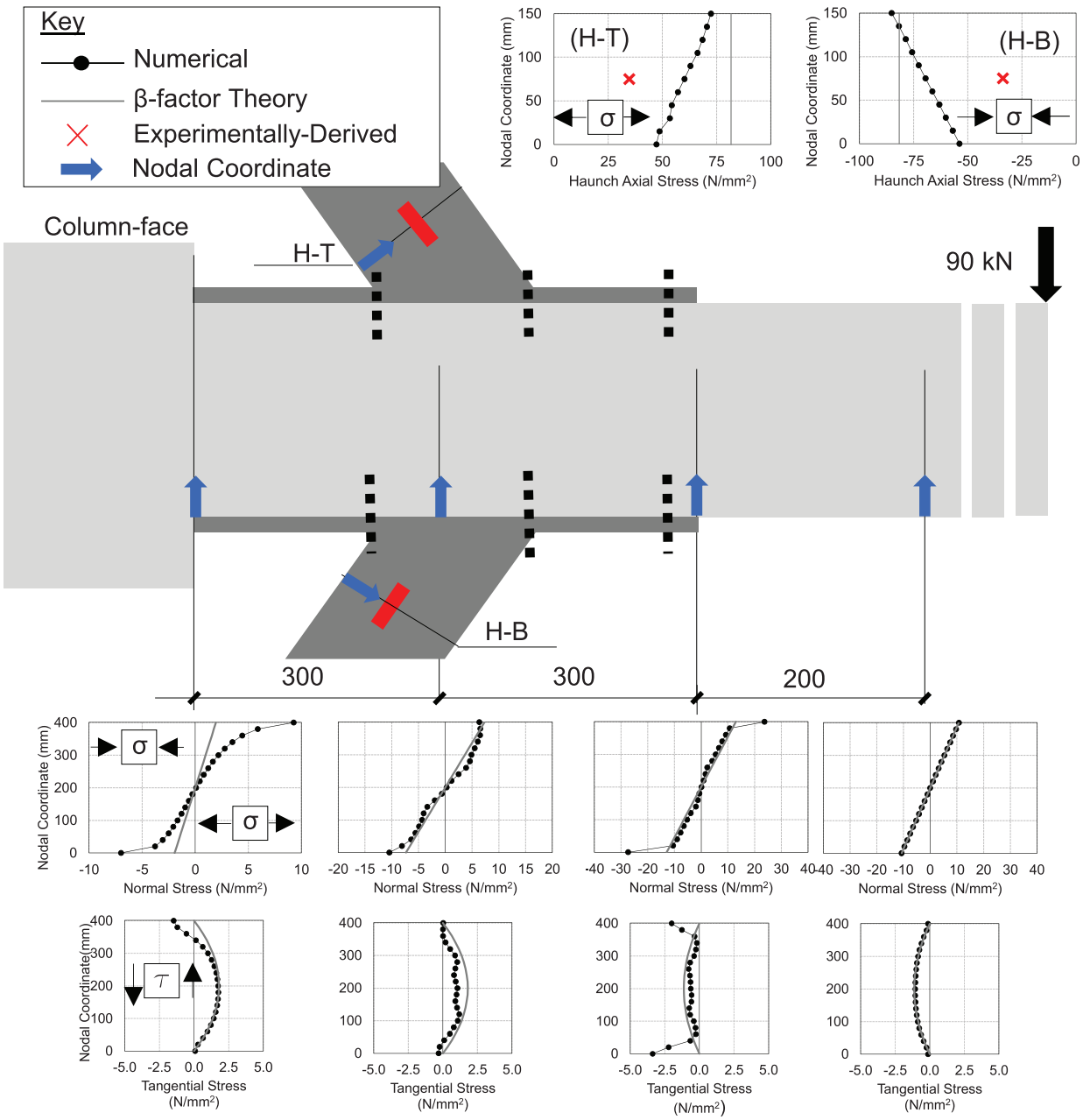


**FIGURE 14** Comparison between numerically derived stresses and $\beta$-factor ones, at relevant beam 's cross-sections of specimen JT1-4, tested by Genesio[29]. (Note. Dimensions are in millimeters. The Reader is referred to the color version of this figure.).

## 4.3 | Summary and design implications

To summarize, $\beta$-factor led an underestimated prediction, with respect to 2D FEM, of joint shear demand for specimen JT1-4. The prediction for specimen THR1 was substantially comparable. Generally, the question is: shall the haunch region be considered either a B-Region, as $\beta$-factor approach assumes, or a D-Region? With regard to this point, by assuming $L'/h_b$ as a conventional slenderness parameter, beam theory would imply $L'/h_b > 2$ according to Schlaich.[40] This is hardly achieved. For example, a maximum value of 2 is found for the experimental database presented in Table 1. Nevertheless, the authors recognize that proposing 2D FEM as a routine procedure to design haunch retrofit may be not computationally optimal. Moreover, the conclusions obtained from the presented benchmarks may suffer lack of generality. As per the former issue, an application of STM is presented in the following Section 5. The latter is generally discussed in Section 6.

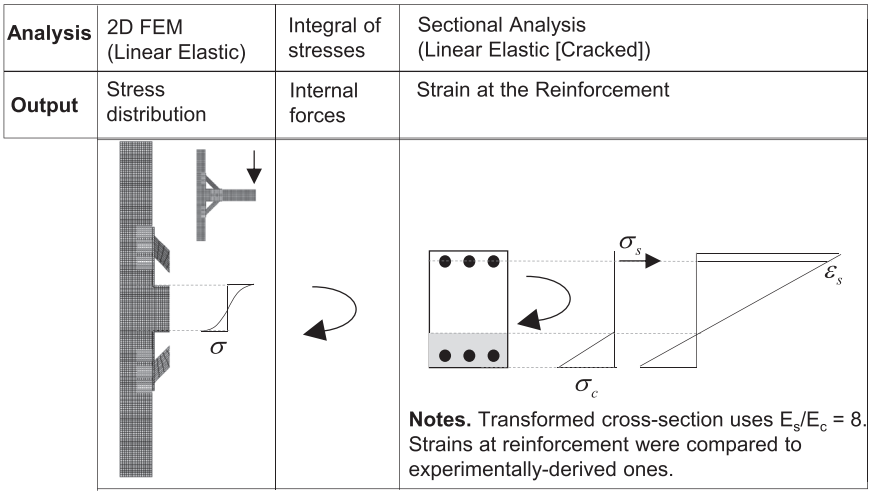


**FIGURE 15** Representation of structural analysis post-processing to get strains at beam's reinforcement.

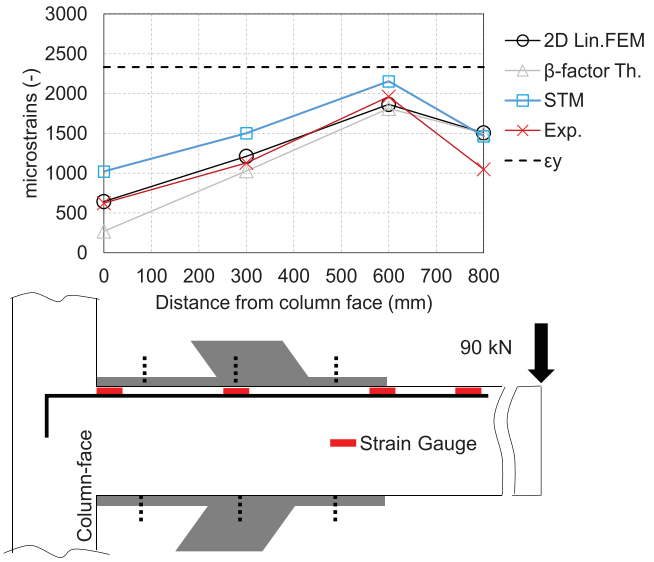


**FIGURE 16** Validation of 2D FEM and STM against experimentally -measured strains of specimen JT1-4, tested by Genesio[29]. (Notes. Experimental data were digitally -derived, from the original publication, using GetData Graph Digitizer software. The Reader is referred to the color version of this figure.

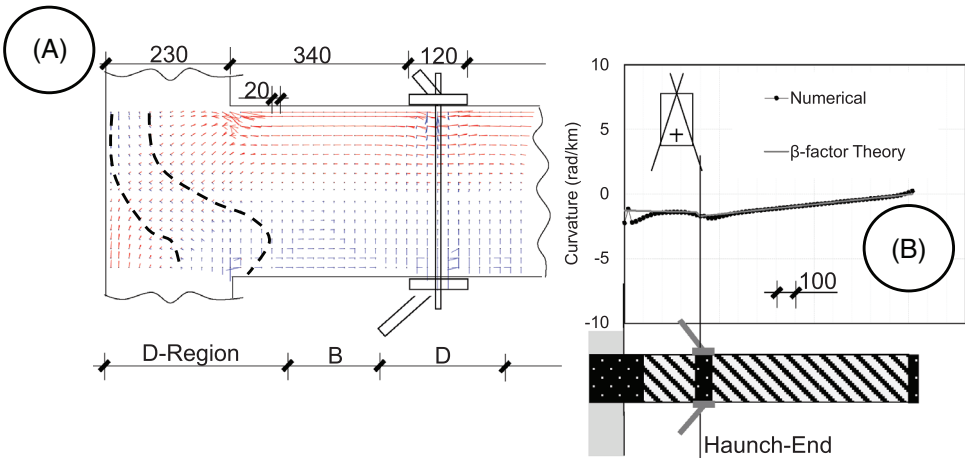


**FIGURE 17** Numerical results of specimen THR1, tested by Pampanin[4]: (A) stress trajectories within the haunch region; (B) numerically derived beam's curvature. (Notes. Dimensions are in millimeters. The Reader is referred to the color version of this figure.).

**TABLE 5** Internal forces of specimen THR1, tested by Pampanin [4].

| ***Beam***[b] | **2D FEM**[a] | | | **β-factor** | |
|---|---|---|---|---|---|
| | $l_s$[c] **(mm)** | ***M*** **(kNm)** | ***V*** **(kN)** | ***M*** **(kNm)** | ***V*** **(kN)** |
| Column face | 0 | 28.2 | −0.4 | 25.2 | −6.0 |
| Intermediate | 100 | 28.0 | −0.4 | 25.8 | −6.0 |
| Intermediate | 200 | 28.2 | −0.4 | 26.4 | −6.0 |
| Intermediate | 300 | 28.3 | −0.4 | 27.0 | −6.0 |
| Haunch end | 400 | 32.5 | −6.0 | 33.6 | 30.0 |
| Clear beam | 500 | 30.8 | 30.0 | 30.8 | 30.0 |
| ***Haunches*** | | | | | |
| | | ***N*** **(kN)** | | ***N*** **(kN)** | |
| (Tension) | | 23.5 | - | 25.5 | |
| (Compression) | | 19.6 | - | 25.5 | |
| ***Joint panel***[d] | | | | | |
| $V_c$ | (kN) | −7.4 | | 0.4 | |
| $T$ | (kN) | 97.8 | | 114.0 | |
| $V_{jh} = T - V_c$ | (kN) | 105.2 | | 113.6 | |

aNumerically derived internal forces are computed as integral of the stresses distributions.
bHogging moments ($M$) are assumed positive. Clockwise shear forces ($V$) are assumed positive.
cDistance of the beam's cross-section from the column face.
dThe sign convention of the horizontal forces acting at the joint panel is shown in Figure 13.

# 5 | APPLICATION OF STM

## 5.1 | Background and Assumptions

STM assumes that the continuous stress field of an RC structure can be studied in a discrete fashion. Essentially, given an RC structure and its load condition, an equivalent truss model is defined such that: (i) equilibrium is satisfied; (ii) the truss' geometry accommodates the stress field, which would characterize the elastic solution; (iii) the resistances are everywhere greater or equal than the corresponding internal forces. The popularity of the method is due to Schlaich who first developed a collection of application examples.[40] Although generally accepted by design guidelines,[41–43] the reference use of uncracked stress field has been debated widely.[44–47] For instance, Ali[45] argued that the design based on linear elastic stress distribution usually results in excessive reinforcement due to stress concentration; on the contrary, excessive use of concrete plasticity may result in premature failure due to crushing. Moreover, as remarked by Fernandez Ruiz,[46] the reinforcement layout itself can impact on the stress distribution.

In the presented investigation, STM was applied to specimens "J T–1" (as-built) and "J T1–4"(retrofitted with haunch) tested by Genesio.[29] The equivalent trusses are shown in Figure 18. Although D-region definition should apply only for the joint panels and haunch regions, the truss model was extended to the whole subassemblage. Additionally, the following assumptions were made:

- The equivalent truss adopted for the as-built condition was statically determinate. Equivalently, haunches were the only source of redundancy in the retrofit condition. The resulting self-weight of the truss is 1.4 ton, which has been considered compliant with respect to the nominal weight of the specimen, that is, 1.5 ton.
- Concrete members were active only in compression, that is, chords and diagonals. The strut width was assumed equal to eight times the longitudinal bars diameters according to ACI guideline.[48] Inclination of the struts, in B-regions, was assumed in a range between 30° and 40° angle, both for the column and the beam.
- Inside the haunch region, two different patterns of compressed struts were studied, that is, HR(i) and HR(ii) in Figure 18. Both the cases assume two diagonal struts formed from the left-top corner of the joint panel to the middle of the compressed haunch plate of beam and column. Such assumption was mainly based on prevailing compression directions

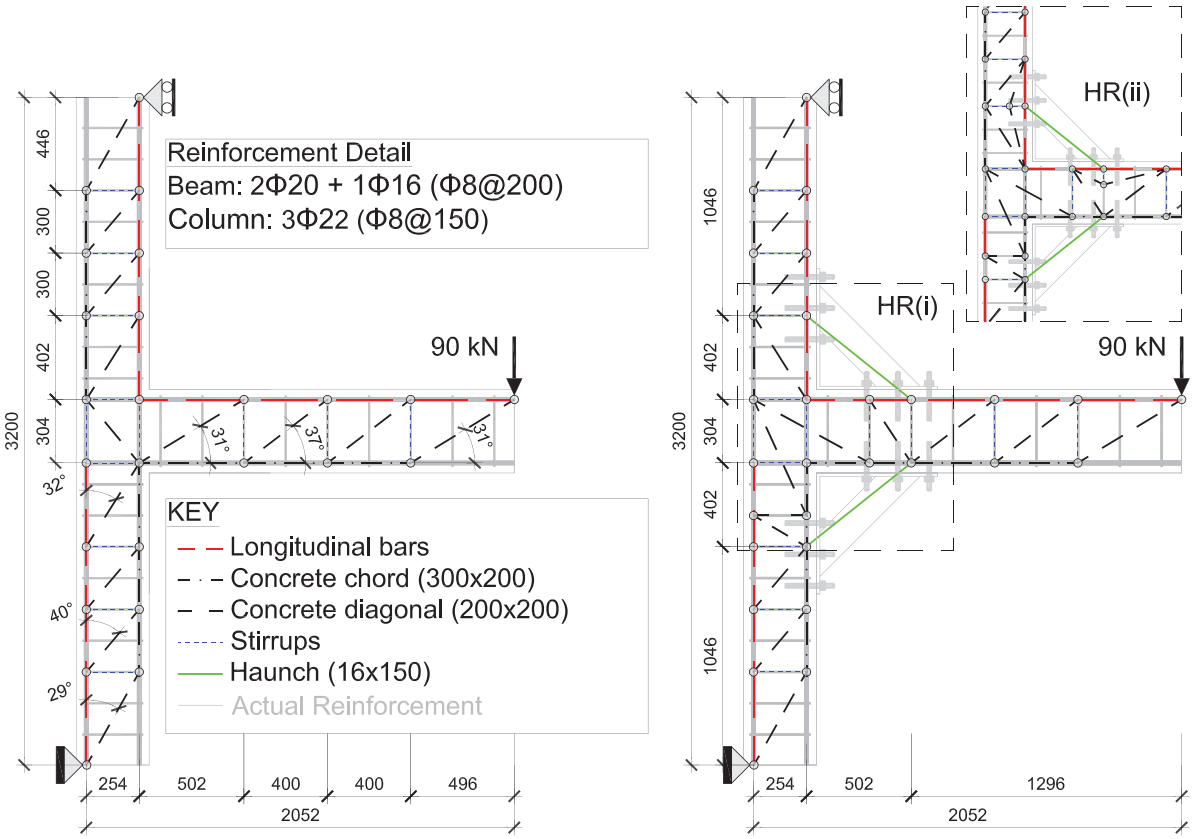


**FIGURE 18** Application of STM equivalent trusses to specimens JT1 (left) and JT1-4 (right) tested by Genesio[29]. (Notes. Dimensions are in millimeters. The Reader is referred to the color version of this figure.) STM, Strut-and-Tie method.

obtained by 2D FEM (see Section 4), which suggested the widening of the diagonal compressive struts through the haunch region. For the case HR(ii), the occurrence of additional struts associated to the pullout behavior of the anchors was investigated. Specifically, the anchors were lumped at a single bar in the vicinity of the middle one. Two nodes were imposed (i) at the attachment with the haunch's diagonal and (ii) at the anchor's unloaded end according to the provision given by Bamonte.[49]

- Reinforcement total area was lumped into an equivalent single layer both for longitudinal bars and stirrups.
- Both concrete and steel were assumed linear-elastic. Load condition was 90-kN point load applied at the beam tip downward. Under such load condition, as already mentioned for 2D FEM, both concrete and steel are supposed to behave linearly within the haunch region while yielding is expected at the haunch end. For the sake of comparison, the same load magnitude was assumed for as-built. Static analysis was carried out, via FEM software RSTAB-8. Releases of nodal moments were applied at all the beam elements.

The authors are aware that a similar procedure was recently employed by Schafei.[50] Indeed, STM was used to discuss experimental results on RC beam–column joint retrofitted by steel angles. However, the model's validation was not clearly demonstrated. In fact, although axial forces of ties were compared with nominal yielding, the experimentally derived stress of reinforcement (converted from strain gauges reading) was only generally mentioned to overcome the yielding threshold.

## 5.2 | Results

Axial force diagrams, obtained by the adoption of STM, are shown in Figure 19 where only the joint region is represented. The values were compared with nominal strengths given in Table 6. As-built condition is characterized by axial force in the top beam's rebar exceeding the yielding threshold, thus, the applied load level (90 kN) overcomes the load carrying capacity. Indeed, joint shear failure was experimentally reached for a load level almost equal to 60 kN as can be inferred

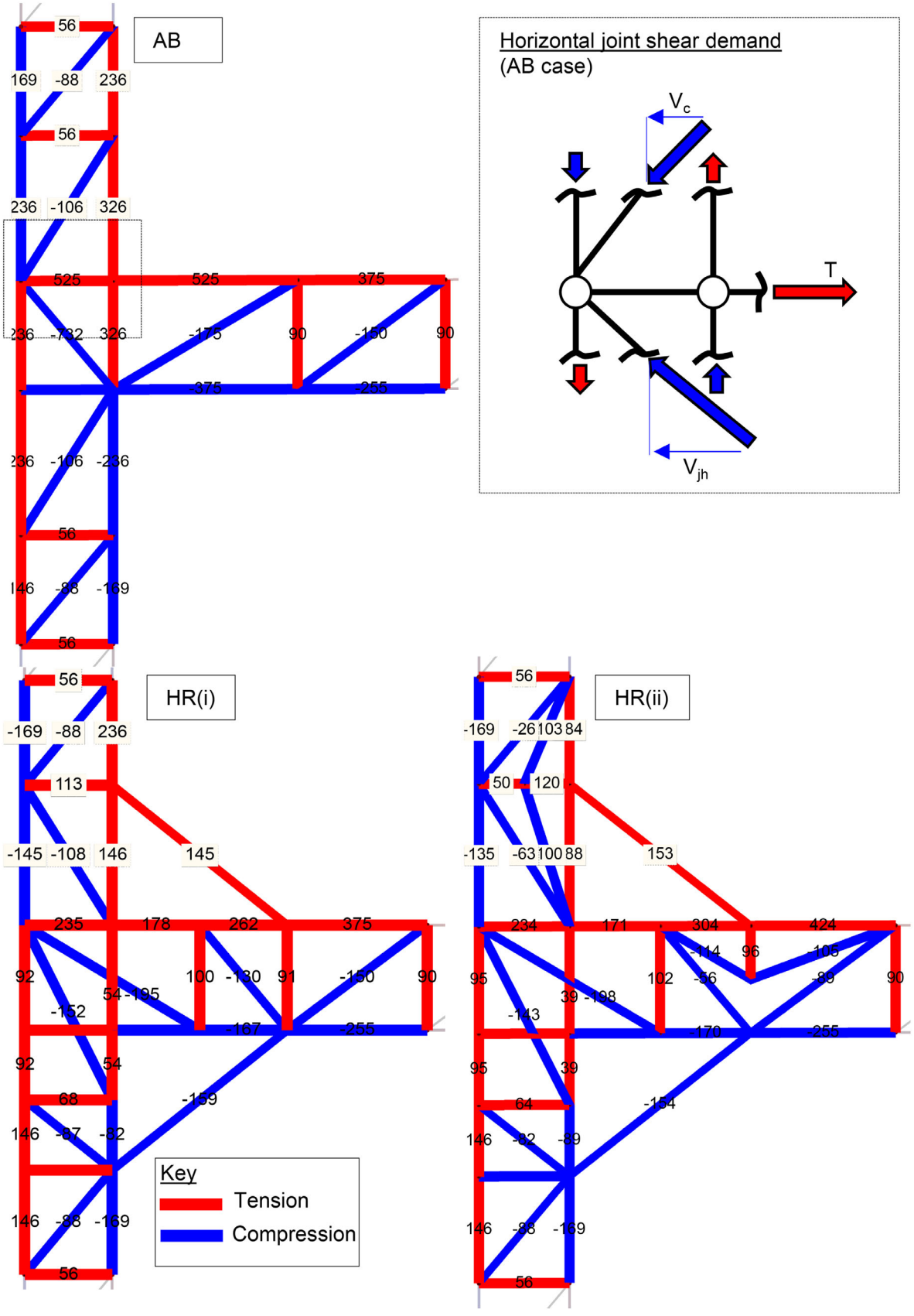


**FIGURE 19** Axial forces of STM equivalent trusses applied to specimens JT1 (AB) and JT1-4 (HR), tested by Genesio[29]. (Notes. Forces are in kilonewton. The Reader is referred to the color version of this figure.) STM, Strut-and-Tie method.

**TABLE 6** Nominal resistances of the STM truss elements applied to specimen JT1-4 [29].

| Element | $A$ ($mm^2$) | $f_y$ or $f_c$ (MPa) | $F$ (kN) |
|---|---|---|---|
| Note | (a) | (b) | (c) |
| Diagonal | 40,000 | 22.4 | 896 |
| Chord | 60,000 | 22.4 | 1344 |
| Stirrups | 201 | 490 | 98 |
| Beam's Rebar | 829 | 490 | 406 |
| Column's Rebar | 1140 | 490 | 559 |
| Haunch | 2400 | 275 | 660 |
| Anchors† | – | – | 105 |

aArea of the truss element.
bNominal strengths: two-third of the cylindrical compressive strength is considered as allowable stress [52] for concrete.
cAxial strength, that is, $F = A \cdot f_y$ or $F = A \cdot f_c$.
† Combined pullout and concrete cone strength for the group of six anchors, evaluated by Genesio[29].

**TABLE 7** STM predicted internal forces of specimens JT1-4, tested by Genesio [29].

| | | 2D FEM[a] | | $\beta$-factor | | Exp./Nom. | STM[e] | | | |
|---|---|---|---|---|---|---|---|---|---|---|
| | | AB[d] | HR | AB | HR | HR | AB(90 kN) | AB(60 kN) | HR(i) | HR(ii) |
| ***Haunches*** | | | $N^h$ (kN) | | $N^h$ (kN) | $N^h$[b] (kN) | | | $N^h$ (kN) | $N^h$ (kN) |
| (Tension) | | – | 124.8 | - | 165.5 | 78.0 | - | | 145.2 | 153.1 |
| (Compression) | | - | 137.3 | - | 165.5 | 81.0 | - | | 159.4 | 154.0 |
| ***Joint panel***[c] | | | | | | | | | | |
| $V_c$ | (kN) | 60.3 | −26.3 | 53.4 | −29.1 | - | 56.2 | 37.5 | - | - |
| $T$ | (kN) | 591.6 | 165.2 | 587.7 | 57.9 | - | 525.0 | 350.0 | 178.1 | 170.5 |
| $V_{jh} = T - V_c$ | (kN) | 531.3 | 191.5 | 534.2 | 87.0 | 279.0[f] | 468.8 | 312.5 | 235.2 | 233.8 |

[a]Results of 2D linear FEM, discussed at Section 4.
[b]Haunch load was obtained from original publication where the values were back-derived from strain gauges glued onto the haunch diagonal.
[c]The sign convention of the horizontal forces acting at the joint panel is shown in Figure 13. STM value of $V_{jh}$ is obtained as horizontal component of the strut's axial force, for example, see Figure 19.
[d]Gray font is used for As-Built (AB), dark font is used for haunch retrofit (HR).
[e]HR(i) and HR(ii) indicate different struts configurations according to Figure 18.
[f]Nominal joint cracking resistance.

from Figure 8. Updated axial forces can be simply obtained by multiplying them times the ratio 60/90 because the truss model is linear. Results are presented in Table 7. The predicted joint shear demand is obtained according to the free-body equilibrium shown in Figure 19. Comparison is made with respect to nominal joint cracking resistance, which is supposed to govern the peak response, for unreinforced joints, rather than concrete compressive failure.[51] As expected, a prone-to-failure condition is obtained. As per the retrofitted joints, differences between HR(i) and HR(ii) are not significant. Axial force diagrams show that concrete chords and diagonals result well below the strength limit, which assumes two-third of the concrete compressive strength as maximum allowable stress.[52,53] Longitudinal reinforcement (top rebar) yielding is obtained at the haunch section. Axial forces in the stirrups resulted at yielding but the result cannot be sustained conclusively due to lack of experimental details. Equivalent anchor, in beam (or column) of model HR(ii), reached a tensile force comparable with respect to the combined pullout and concrete cone resistance of the anchors group (six anchors) although the failure was not experimentally observed. To further validate the STM model, the axial force of the beam's top rebar was converted into strain by dividing the elastic stiffness. Results are presented in Figure 16 and Table 4. For the sake of synthesis, only HR(i) results are discussed. Predicted strains are larger than experimentally derived ones. Nevertheless, from the specific assessment prospective assumed in this paper, which targets the joint shear demand, it is proved that a conservative estimate is obtained as can be derived from Table 7.

# 6 | LIMITATIONS

## 6.1 | The use of 2D linear FEM

The validity of the $\beta$-factor approach to predict joint shear demand for beam—column joint retrofitted via haunch retrofit was questioned for specimen JT1-4, tested by Genesio.[29] Violation of B-region hypothesis was demonstrated by using 2D linear-elastic FEM. Of course, linear material behavior does not represent the cracked condition of concrete. Similar assumption, though, is made to define the $\beta$-factor. In fact, beam's (or column) flexibility coefficients, in the Equation (2), are based on linear-elastic flexural modulus. Another aspect, which may rise doubts, is the adopted comparison between 2D plane stress FEM and $\beta$-factor approach, which assumes the beam theory. On this subject, inspiration was taken from the notorious "Cantilever" example defined by Carr[54] and extended by MacNeal.[55] In this case, FEM performances of different elements (either triangular or quadrilateral) are tested against elasticity solution, which coincides with beam theory with the exception of clamp's proximity where the "De-Saint Venant Principle"[56] is violated. Generally, the comparison employed the displacement field outside the disturbed end. In this light, the presented investigation assumed a similar criterion, that is, comparison of curvatures outside the haunch region was given. Nonetheless, the authors recognize that their conclusions on stress field can be only partial because they are based on specific benchmark geometries. Further studies are needed which should, for example, assume single haunch and refined model for anchorages' pullout.[57]

## 6.2 | The use of STM

Among infinite equilibrated solutions, only few equivalent trusses were studied. Modeling criteria assumed (i) statically determinate truss for the as–built condition and (ii) compressive field angle in a range between 30° and 40°. The geometry of concrete struts inside the haunch region was qualitatively oriented according to the results of 2D FEM linear analysis. However, its adequacy needs to be investigated further possibly by applying optimization criteria.[45,58] Contrary to the common use of STM, which addresses the design of the reinforcement for new RC structures under monotonic loads, the presented investigation proposes it as an assessment tool for seismic conditions. In this respect, the assumed rigid-plastic behavior of concrete may be too optimistic. In fact, concrete should retain its maximum stress for strains of arbitrary magnitude.[59] However, this is hardly achieved at the joint panel because (i) cracked concrete is notoriously subjected to compressive strength decay[60] and (ii) degradation of shear strength is expected for cyclic condition.[61] To solve the issue, the allowable concrete strength (assumed equal to two-third of the concrete strength[53] for the sake of simplicity) should be reduced further. As noted above for 2D FEM, also the presented application of STM does not possess enough validity to be generalized. For example, trusses were tailored aiming at representing beam's hogging behavior, thus, they are not suitable to represent sagging condition, that is, both the concrete diagonals and the compressed chords need to be re-assigned. Finally, three-dimensional STM should be applied insofar as haunch retrofit was extended to corner joints (bi-axially loaded) or joints with transverse beam. In this respect, the authors will present in a future paper a validation of the model supported by their experimental results.

# 7 | CONCLUSIONS

This paper studied the stress field of RC beam–column joints retrofitted with haunch retrofit. Two benchmarks were selected among specimens surveyed from literature. They represent two extreme cases with respect to the validity of the $\beta$-factor definition, which is the state-of-the-art of structural analysis for haunch retrofit. Internal forces, obtained by 2D FEM, assuming linear-elastic materials, were compared to $\beta$-factor approach. An application of STM was proposed as an easy-to-handle alternative to 2D FEM. Validation against experimental results was partly possible by comparing, for one of the selected benchmarks, experimentally derived strains to numerically derived ones. Being the principal scope of haunch retrofitting the decrease of shear demand at the joint, such parameter was considered as a key output for the comparison. In this instance, three are the most consistent findings. First, $\beta$-factor applies linear strains (beam theory) in the haunch region. Such hypothesis was proved to be violated for haunches with stiff diagonal and extended flat plates. In this case, stresses (and strains) deviate from linear distribution across the cross-section's depth. As a result, the $\beta$-factor prediction of bending moment at column–face (and in its vicinity) could be not valid. In this regard, by integrating stress

profile resulting from 2D linear FEM, larger values of bending moment were obtained. Conversely, shear forces showed nonsignificant differences. Second, as a consequence of the previous finding, $\beta$-factor gave almost one half of the joint shear demand if compared with 2D linear FEM. Such underestimation may be not acceptable in practical retrofit design circumstance. Third, STM proved to be an appropriate method to evaluate the internal forces of beam–column joints retrofitted with haunches. The adopted truss schemes were derived on the basis of prevailing compression directions inferred from 2D linear FEM. Conservative estimates of joint shear demand (up to 25%) were obtained if compared to 2D FEM.

## AUTHOR CONTRIBUTIONS

*Conceptualization*: Angelo Marchisella and Giovanni Muciaccia. *Methodology*: Angelo Marchisella and Giovanni Muciaccia. *Software*: Angelo Marchisella. *Validation*: Angelo Marchisella. *Data curation*: Angelo Marchisella. *Writing—original draft and reviews*: Angelo Marchisella. *Writing—reviews*: Giovanni Muciaccia. All authors have read and agreed to the published version of the manuscript.

## ACKNOWLEDGMENTS

The authors have nothing to report.

## DATA AVAILABILITY STATEMENT

The data that support the findings of this study are available from the corresponding author upon reasonable request.

## ORCID

*Angelo Marchisella* https://orcid.org/0000-0001-9919-6370
*Giovanni Muciaccia* https://orcid.org/0000-0002-1224-5449

## REFERENCES

1. Civjan SA, Engelhardt MD, Gross JL. Retrofit of pre-northridge moment-resisting connections. *J Struct Eng*. 2000;126(4):445-452. https://doi.org/10.1061/(asce)0733-9445(2000)126:4(445)
2. Yu QS, Gross JL. Seismic rehabilitation design of steel moment connection with welded haunch. *J Struct Eng (United States)*. 2000;126:69-78.
3. Pampanin S, Christopoulos C. Non invasive retrofit of existing RC frames designed for gravity loads only. In: Proceedings of the fib Symposium 2003: Concrete Structures in Seismic Regions. 2003:382-383.
4. Pampanin S, Christopoulos C, Chen TH. Development and validation of a metallic haunch seismic retrofit solution for existing under-designed RC frame buildings. *Earthq Eng Struct Dyn*. 2006;44:657-675. https://doi.org/10.1002/eqe
5. Chen Th, Pampanin S. *Retrofit Strategy of Non-seismically Designed Frame Systems Based on a Metallic Haunch System*. MSc thesis. University of Canterbury; 2006.
6. Pohoryles DA, Melo J, Rossetto T, Varum H, Bisby L. Seismic retrofit schemes with FRP for deficient RC beam-column joints: State-of-the-art review. *J Compos Constr*. 2019;23(4):03119001. https://doi.org/10.1061/(asce)cc.1943-5614.0000950
7. Marchisella A, Muciaccia G, Sharma A, Eligehausen R. Experimental investigation of 3D RC exterior joint retrofitted with FFHR. *Eng Struct*. 2021;239:112206. https://doi.org/10.1016/j.engstruct.2021.112206
8. Marchisella A. *Seismic Assessment of Existing 3D RC Beam-Column Joints and Retrofit with Fully Fastened Haunch*. Phd thesis. Politecnico di Milano; 2022.
9. Ahmad N, Akbar J, Rizwan M, Alam B, Khan AN, Lateef A. Haunch retrofitting technique for seismic upgrading deficient RC frames. *Bull Earthq Eng*. 2019;17(7):3895-3932. https://doi.org/10.1007/s10518-019-00638-9
10. Sharbatdar M, Kheyroddin A, Emami E. Cyclic performance of retrofitted reinforced concrete beam-column joints using steel prop. *Constr Build Mater*. 2012;36:287-294. https://doi.org/10.1016/j.conbuildmat.2012.04.115
11. Kheyroddin A, Emami E, Khalili A. RC Beam-column connections retrofitted by steel prop: Experimental and analytical studies. *Int J Civ Eng*. 2020;18(5):501-518. https://doi.org/10.1007/s40999-019-00481-8
12. AISC. *Modification of Existing Welded Steel Moment Frame Connections for Seismic Resistance*. Technical report. American Institute of Steel Construction; 1999.
13. Zhao H, Shi G, Chen X, Xiao T. Numerical simulation and mechanical model of steel beam-to-column joints retrofitted by haunches. *J Constr Steel Res*. 2021;185:106858. https://doi.org/10.1016/j.jcsr.2021.106858
14. Zabihi A, Tsang HH, Gad EF, Wilson JL. Seismic retrofit of exterior RC beam-column joint using diagonal haunch. *Eng Struct*. 2018;174:753-767. https://doi.org/10.1016/j.engstruct.2018.07.100
15. Veismoradi S, Mohamad Mahdi Yousef-beik S, Zarnani P, Quenneville P. Seismic strengthening of deficient RC frames using self-centering friction haunches. *Eng Struct*. 2021;248:113261. https://doi.org/10.1016/j.engstruct.2021.113261
16. Wang B, Zhu S, Xu YL, Jiang H. Seismic retrofitting of non-seismically designed RC Beam-column joints using buckling-restrained haunches: design and analysis. *J Earthq Eng*. 2018;22(7):1188-1208. https://doi.org/10.1080/13632469.2016.1277441

17. Sharma A, Eligehausen R. Numerical modeling of joints retrofitted with haunch retrofit solution. *ACI Struct J*. 2014;111(4):861-872. https://doi.org/10.14359/51686737
18. Tasligedik AS, Akguzel U, Kam WY, Pampanin S. Strength hierarchy at reinforced concrete beam-column joints and global capacity. *J Earthq Eng*. 2018;22(3):454-487. https://doi.org/10.1080/13632469.2016.1233916
19. Ahmad N. Force-based seismic design of steel haunch retrofit for RC frames. *Earthq Struct*. 2021;20(2):133-148. https://doi.org/10.12989/eas.2021.20.2.133
20. Akbar J, Ahmad N, Alam B. Response modification factor of haunch retrofitted reinforced concrete frames. *J Perform Constr Facil*. 2020;34(6):04020115. https://doi.org/10.1061/(ASCE)CF.1943-5509.0001525
21. Mwafy AM, Elnashai AS. Calibration of force reduction factors of RC buildings. *J Earthq Eng*. 2002;6(2):239-273. https://doi.org/10.1080/13632460209350416
22. Sharma A. *Seismic Behavior and Retrofitting of RC Frame Structures with Emphasis on Beam Column Joints. Experiments and Numerical Modeling*. Phd thesis. University of Stuttgart; 2013.
23. Sharma A, Eligehausen R, Reddy GR. A new model to simulate joint shear behavior of poorly detailed beam-column connections in RC structures under seismic loads, Part I: exterior joints. *Eng Struct*. 2011;33(3):1034-1051. https://doi.org/10.1016/j.engstruct.2010.12.026
24. Sharma A, Reddy GR, Eligehausen R. *Joint Model to Simulate Inelastic Shear Behavior of Poorly Detailed Exterior and Interior Beam-Column Connections Reinforced with Deformed Bars Under Seismic Excitations*. Technical report. Bhabha Atomic Research Centre; 2009.
25. Muto K. *Seismic Analysis of RC Buildings*. Technical report. Tokyo Shokoku-ska Publishing Company; 1965.
26. Caterino N, Cosenza E. Approximate methods to evaluate storey stiffness and interstory drift of RC buildings in seismic area. *Struct Eng Mech*. 2013;46(2):245-267. https://doi.org/10.12989/sem.2013.46.2.245
27. Elwood KJ. Effective stiffness of reinforced concrete columns. *ACI Struct J*. 2010;107(3):372-373.
28. Emami E, Kheyroddin A, Sharbatdar MK. Experimental and analytical investigations of reinforced concrete beam-column joints retrofitted by single haunch. *Adv Struct Eng*. 2020;23(15):3171-3184. https://doi.org/10.1177/1369433220922493
29. Genesio G. *Seismic Assessment of RC Exterior Beam -Column Joints and Retrofit with Haunches Using Post-Installed Anchors*. Phd thesis. University of Stuttgart; 2012.
30. Paulay T, Priestley N. *Seismic Design for Concrete and Masonry Buildings*. Wiley; 1992.
31. Truong GT, Dinh NH, Kim JC, Choi KK. Seismic performance of exterior RC beam-column joints retrofitted using various retrofit solutions. *Int J Concr Struct Mater*. 2017;11(3):415-433. https://doi.org/10.1007/s40069-017-0203-x
32. ACI. *318-19 Building Code Requirements for Structural Concrete and Commentary*. American Concrete Institute; 2019
33. Wilson EL, Taylor RL, Doherty W, Ghaboussi J. Incompatible Displacement Models. In: *Numerical and Computer Methods in Structural Mechanics*. Academic Press; 1973:43-57.
34. FIB. fib Model Code for Concrete Structures 2010. International Federation for Structural Concrete; 2013.
35. CSI. CSI Analysis Reference Manual. For SAP2000, ETABS, SAFE, CsiBridge [Version 2017]. Technical report. 2017.
36. Hinton E. Local and global smoothing of discontinuous finite element functions. *Int J Numer Methods Eng*. 1974;8:461-480.
37. Schlaich J, Schafer K. Design and detailing of structural concrete using strut-and-tie models. *Struct Eng*. 1991;69(6):113-125.
38. Payen DJ, Bathe KJ. The use of nodal point forces to improve element stresses. *Comput Struct*. 2011;89(5-6):485-495. https://doi.org/10.1016/j.compstruc.2010.12.002
39. Collins MP, Mitchell D. *Prestressed Concrete Structures*. Prentice-Hall International; 1991.
40. Schlaich J, Schafer K, Jennewein M. Toward a consistent design of structural concrete. *PCI J*. 1987;32:74-150. https://doi.org/10.15554/pcij.05011987.74.150
41. ACI. *PRC-445.2-21: Strut-and-Tie Method Guidelines for 318-19 - Guide*. ACI; 2021.
42. Breen J, Bergmeister K, Jirsa JO, Kreger M. *Detailing For Structural Concrete*. 1993.
43. FIB. Bulletin 100 - Design and Assessment with strut-and-tie Models and Stress Fields: From Simple Calculations to Detailed Numerical Analysis. International Federation for Structural Concrete; 2021
44. Muttoni A, Schwarz MJ. *Design of Concrete Strucutres with Stress Fields*. Birkhauser Verlag; 1997.
45. Ali M, White RN. Automatic generation of truss models for the optimal design of reinforced concrete structures. *ACI Struct J*. 2001;(98):431-442.
46. Fernández Ruiz M, Muttoni A. On development of suitable stress fields for structural concrete. *ACI Struct J*. 2007;104(4):495-502. https://doi.org/10.14359/18780
47. Lourenço MS, Almeida J. Adaptive stress field models: formulation and validation. *ACI Struct J*. 2013;110(6):1116-1119.
48. ACI. *445R-99 Recent Approaches to Shear Design of Structural Concrete*.
49. Bamonte P, Gambarova PG, Invernizzi R. Bond role in strut-and-tie systems modelling reinforced-concrete members. *Eng Struct*. 2020;209:109946. https://doi.org/10.1016/j.engstruct.2019.109946
50. Shafaei J, Nezami S. Effect of different size of joint enlargement on seismic behavior of gravity load designed RC beam-column connections. *Struct Des Tall Build*. 2019;28(14):1-27. https://doi.org/10.1002/tal.1653
51. Fardis MN. *Seismic Design, Assessment and Retrofitting of Concrete Buildings*. Springer; 2009.
52. Kuchma D, Yindeesuk S, Nagle T, Hart J, Lee HH, Windisch A. Experimental validation of strut-and-tie method for complex regions. *ACI Struct J*. 2009;106(4):552.
53. Marti P. Basic tools of reinforced concrete beam design. *ACI Struct J*. 1985;82(4):46-56.
54. Carr AJ. *A Refined Finite Element Analysis of Thin Shell Structures Including Dynamic Loadings*. Phd thesis. University of California; 1967.

55. MacNeal R. A proposed Standard set of problems to test finite element accuracy. *Finite Elem Anal Des*. 2004;40(11):1445-1451. https://doi.org/10.1016/j.finel.2003.10.001
56. Goodier JN. A general proof of Saint-Venant's principle. *Lond Edinb Dublin Philos Mag J Sci*. 1937;23(155). https://doi.org/10.1080/14786443708561833
57. Bokor B, Sharma A, Hofmann J. Spring modelling approach for evaluation and design of tension loaded anchor groups in case of concrete cone failure. *Eng Struct*. 2019;197:109414. https://doi.org/10.1016/j.engstruct.2019.109414
58. Biondini F, Bontempi F, Malerba PG. Optimal strut-and-tie models in reinforced concrete structures. Computer Assisted Mechanics and Engineering Sciences. 1999;6(3-4):280-293.
59. Exner H. On the effectiveness factor in plastic analysis of concrete. *IABSE Colloquium, Copenhagen*. 1979;29:35-42.
60. Vecchio FJ, Collins MP. The modified compression-field theory for reinforced concrete elements subjected to shear. *ACI Struct J*. 1986;83(2):219-231. https://doi.org/10.14359/10416
61. Biskinis D, Fardis MN. Cyclic shear resistance model for Eurocode 8 consistent with the second-generation Eurocode 2. *Bull Earthq Eng*. 2020;18(6):2891-2915. https://doi.org/10.1007/s10518-020-00807-1
62. Kanchanadevi A, Ramajaneyulu K. Non-invasive hybrid retrofit for seismic damage mitigation of gravity load designed exterior beam–column sub-assemblage. *J Earthq Eng*. 2019:1-26. https://doi.org/10.1080/13632469.2019.1592790
63. Genesio G, Eligehausen R, Sharma A, Pampanin S. Application of post-installed anchors for seismic retrofit of RC beam-column joints: design and validation. In: Concrete Repair, Rehabilitation and Retrofitting III - Proceedings of the 3rd International Conference on Concrete Repair, Rehabilitation and Retrofitting, ICCRRR 2012. 2012:1202-1208. https://doi.org/10.1201/b12750-201
64. Bentz EC. *Sectional Analysis of Reinforced Concrete Members*. Phd dissertation. University of Toronto; 2000.


**How to cite this article:** Marchisella A, Muciaccia G. Haunch retrofit of RC beam–column joints: Linear stress field analysis and Strut-and-Tie method application. *Earthquake Engng Struct Dyn*. 2023;1-25. https://doi.org/10.1002/eqe.3921